UNLV | UNIVERSITY LIBRARIES

UNLV Theses, Dissertations, Professional Papers, and Capstones

5-1-2013

Strategic Electronic Property Control of Self-Assembling Pyrazine-Acenes

Lacie Brownell
University of Nevada, Las Vegas

Follow this and additional works at: https://digitalscholarship.unlv.edu/thesesdissertations

Part of the Organic Chemistry Commons, and the Semiconductor and Optical Materials Commons

Repository Citation

Brownell, Lacie, "Strategic Electronic Property Control of Self-Assembling Pyrazine-Acenes" (2013). *UNLV Theses, Dissertations, Professional Papers, and Capstones*. 1807.
http://dx.doi.org/10.34917/4478203

This Thesis is protected by copyright and/or related rights. It has been brought to you by Digital Scholarship@UNLV with permission from the rights-holder(s). You are free to use this Thesis in any way that is permitted by the copyright and related rights legislation that applies to your use. For other uses you need to obtain permission from the rights-holder(s) directly, unless additional rights are indicated by a Creative Commons license in the record and/or on the work itself.

This Thesis has been accepted for inclusion in UNLV Theses, Dissertations, Professional Papers, and Capstones by an authorized administrator of Digital Scholarship@UNLV. For more information, please contact digitalscholarship@unlv.edu.

STRATEGIC ELECTRONIC PROPERTY CONTROL OF SELF-ASSEMBLYING PYRAZINE-ACENES

by

Lacie V. Brownell

Bachelor of Science in Biochemistry

University of Nevada, Las Vegas

2008

A thesis submitted in partial fulfillment

of the requirement for the

Master of Science in Chemistry

Department of Chemistry

College of Sciences

The Graduate College

University of Nevada, Las Vegas

May 2013

THE GRADUATE COLLEGE

We recommend the thesis prepared under our supervision by

Lacie Brownell

entitled

Strategic Electronic Property Control of Self-Assemblying Pyrazine-Acenes

be accepted in partial fulfillment of the requirements for the degree of

Master of Science in Chemistry
Department of Chemistry

Dong-Chan Lee, Ph.D., Committee Chair

David Hatchett, Ph.D., Committee Member

Kathleen Robins, Ph.D., Committee Member

Monika Neda, Ph.D., Graduate College Representative

Tom Piechota, Ph.D., Interim Vice President for Research &
Dean of the Graduate College

May 2013

ABSTRACT

Strategic Electronic Property Control of Self-Assembling Pyrazine-Acenes

by

Lacie V. Brownell

Dr. Dong-Chan Lee, Exam Committee Chair
Associate Professor of Chemistry
University of Nevada- Las Vegas

Control of electronic properties in organic semiconductor materials is essential for electro-optical applications such as field-effect transistors, light-emitting diodes, and photovoltaic devices. This work is focused on two systems that highlight different approaches for the manipulation of electronic properties: (I) the development of electron-deficient (n-type) materials by selective lowering of E_{LUMO} and (II) low energy gap materials by controlling both E_{LUMO} and E_{HOMO}.

To specifically lower $E_{LUMO,}$ a pyrazine-acene π-platform was extended using electron-withdrawing moieties. These include: pyridine, pyrazine, and benzothiadiazole (system I). From the base pyrazine-acene, the most significant change in E_{LUMO} of 0.83 eV was observed with benzothiadiazole π-extender, while pyridine and pyrazine lowered E_{LUMO} by 0.15 eV and 0.42 eV, respectively. E_{HOMO} was relatively unaffected by these π-extenders.

The mechanism for E_{LUMO} control in this system was illustrated by theoretical evaluation. We found that the LUMO orbital localized on the more electron deficient part of the pyrazine-acene including the π-extenders, while the HOMO orbital localized on the more electron rich portion, away from the π-extenders. This enabled us to achieve specific control of E_{LUMO} depending on the type of π-extenders.

To achieve low energy gap (E_{gap}) materials, structures containing electron rich (donor) thiophene attached to an electron deficient (acceptor) pyrazine-acene π-core were synthesized as system II. The effects of planarity, type of solubilizing side group (i.e. alkyl vs. alkoxy), and type of pyrazine-acene π-core on E_{gap} have been evaluated both experimentally and theoretically. Extension of the π-core with a thiadiazole moiety further enhanced the electron deficiency of the acceptor part of the molecule resulting in a decrease of E_{LUMO} from -3.32 eV to -3.90 eV. An impressive E_{gap} compression of 1.21 eV was achieved with this donor-acceptor configuration, which is rare for a small molecule.

Through systematic theoretical investigation, it was found that the dihedral angle between the pyrazine-acene acceptor and the thiophene donor affects E_{HOMO} rather than E_{LUMO}. This was also supported experimentally with planar and nonplanar systems.

Most of the compounds of system I and II assembled into one-dimensional (1D) fibers with a width of 10 nm to 2μm via organogelation, phase-transfer assembly, or simple-drop casting. This demonstrates the utility of the presented molecular design in generating beneficial self-assemble fibers.

ACKNOWLEDGEMENTS

First of all, I'm deeply thankful for all the patience that my advisor, Dr. Lee, has had with me all these years. Not only have I gained incredibly useful knowledge that has allowed me to grow as a scientist, but I have also been given lessons that have helped me grow as a person. For that, I will be forever grateful as I know that is has not been an easy task.

I am very thankful to have such great committee members: Dr. Robins, Dr. Hatchett, and Dr. Neda. It has been comforting to know that their doors are always open to questions, or even just friendly conversations. Being surrounded by people that genuinely care about their work and the students around them has truly made this a special place to study. Furthermore, financial support from NSF Award DMR-0846479 is much appreciated.

Without the help of Dr. Ich Tran, AFM studies would not be possible. Likewise, Dr. Paul Forster ran crystallographic studies important to the characterization of compounds presented in this thesis. The guidance of Dr. Longzhou Ma during TEM studies is greatly appreciated.

I'd also like to extend my gratitude towards my fellow students. Special thanks to Tae soo Jo and Hana Yang for being great supportive friends that I could always count on. Renee de los Angeles has helped me tremendously with lab work, and always has a good attitude which is very much appreciated. Kyoungmi Jang was a previous lab mate that was also a good friend. I am thankful for everything she taught me in the lab, and at great Korean restaurants.

Outside of the department, I have also been blessed with an amazing support system. My dearest climbing partners, Donna and Matt are unbelievably understanding, and always willing to go get on something big to make the weekend worthwhile. By far, Jacob and Michael have listened to me complain about, or praise my graduate studies more than anyone else, and I am truly grateful to have a friends like them.

Last, but certainly not least, my family. Without them, I certainly would not be here in the first place. Thanks will never be sufficient enough for everything they have provided me with.

TABLE OF CONTENTS

ABSTRACT…….iii

ACKNOWLEDGEMENTS……..v

LIST OF TABLES……ix

LIST OF FIGURES……..……x

LIST OF SCHEMES……xii

CHAPTER 1 CONTROL OF E_{LUMO} BY EXTENSION OF THE PYRAZINE-ACENE π-CORE

1.1 Introduction……..…….…….1

1.2 Experiments……..……..3

1.2.1 Instrumentation……....3

1.2.2 Synthetic Procedures……....4

1.2.3 Organogelation……..…7

1.2.4 Gelling Temperature (T_{gel})…….……..7

1.2.5 Phase Transfer (PT) Assembly……8

1.3 Results and Discussion…….8

1.3.1 Synthesis……..8

1.3.2 Physical Properties……11

1.3.2.1 Optical Properties……11

1.3.2.2 Electrochemical Properties……..13

1.3.3 Theoretical Evaluation…….…..15

1.3.4 Assembly Properties……..20

1.4 Conclusion……..25

Chapter 2 COMPRESSION OF E_{gap} USING A DONOR-ACCEPTOR SYSTEM

2.1 Introduction…….……. 27

2.2 Experiments……..…… 30

2.2.1 Instrumentation……..….. 30

2.2.2 Synthetic Procedures……..…..31

2.2.3 Cast Film……..……. 37

2.2.4 Precipitation……..... 37

2.2.5 Phase Transfer (PT) Assembly…….37

2.3 Results and Discussion……..…... 37

2.3.1 Synthesis……..… 37

2.3.2 Physical Properties……..……..…41

2.3.2.1 Optical Properties……...……41

2.3.2.2 Electrochemical Properties……..45

2.3.2.3 Theoretical Evaluation……..…….47

2.3.2.4 Assembly Properties……..…… 54

2.4 Conclusion……..…….58

APPENDIX & SUPPORTING INFORMATION……. 60

REFERENCES……...……. 70

VITA……..…….. 80

LIST OF TABLES

Table 1.1 Molar absorbtivity and Fluorescence quantum efficiency of System I…...… 12

Table 1.2 Summary of System I Electronic Properties.....16

Table 1.3 Gelation test of System I compounds…….. 21

Table 2.1 Molar absorbtivity and Fluorescence quantum efficiency of System II…..…45

Table 2.2 Experimental and theoretical[a] electronic properties of the **PA-TH**s..... 47

Table 2.3 Dihedral angles of thiophene-pyrazine-acenes with thiophene-S facing downward, interacting with pyrazine-N……..... 49

LIST OF FIGURES

Figure 1.1 Pyrazine-acenes with π-extenders (system I). [a]reference **PA** with peripheral cyano substituent. [b]synthetically unavailable and only presented with theoretical data.....3

Figure 1.2 UV-Vis spectra of system I……..... 11

Figure 1.3 Cyclic voltammograms of system I……..... 14

Figure 1.4 Graphical representation of system I electronic properties. [a] reference 23, [b] Synthetically unavailable. Numerical values are provided in Table 2……..... 17

Figure 1.5 Correlation between E_{LUMO} obtained experimentally and theoretically……..…....18

Figure 1.6 Molecular orbital diagrams of system I: (a) **CN-PA**, (b) **PA-PYZ**, (c) **PA-BTD**, (d) **PA-BTD-Br**, and (e) **PA-BTD-TIPSA**..... 20

Figure 1.7 Polarized Optical Microscopy of (a) **CN-PA** from PT; **PA-PY** (10 mM cyclohexane gel); (c) **PA-PYZ** (26 mM TCE gel); (d) **PA-BTD-Br** (4 mM partial gel)……..…..…22

Figure 1.8 AFM images of (a and e) **CN-PA** assembled by the PT method (2 mL of 1 mM methylene chloride solution/2 mL MeOH); (b and f) cyclohexane gel of **PA-PY** (10 mM) dispersed in hexane; (c and g) xerogel from cyclohexane gel of **PA-PYZ** (4mM); (d and h) partial gel of **PA-BTD-Br** from $CHCl_3$ (4 mM). Image size: (a) 20 μm × 20 μm, (b) 10 μm ×10 μm, (c) 20 μm × 20 μm, (d) 50 μm × 50 μm, (e) 10 μm ×10 μm, (f) 1 μm ×1 μm, (g) 5 μm ×5 μm, and (h) 5 μm ×5 μm……...……..…23

Figure 1.9 Partial crystal structure of **PA-BTD-TIPSA**……..……24

Figure 1.10 UV-Vis spectra of (a) **PA-PY** and (b) **PA-PYZ** in the gel and solution state……..……..…….. 25

Figure 2.1 Low E_{gap} compounds based on a thiophene donor and pyrazine-acene acceptor (system II)……..…29

Figure 2.2 Chloroform solutions of (from left to right): **P-TH-OC10**, **P-TH-C10**, **BP-TH-OC16**, **TD-P-TH-C10**, **TD-P-CH$_3$TH-C10**, **TD-P-diTH-C10**, and **TD-BP-TH-OC16**……..….. 42

Figure 2.3 UV-Vis spectra of the system II molecules: (a) **P-TH-OC10**, (b) **P-TH-C10**, (c) **BP-TH-OC16**, (d) **TD-P-TH-C10**, (e) **TD-P-diTH-C10**, (f) **TD-P-MeTH-C10**, and (g) **TD-BP-TH-OC16** in $CHCl_3$……..44
Figure 2.4 Cyclic voltammograms of **PA-TH**s…….....46
Figure 2.5 **PA-TH**s used for theoretical evaluation……..… 48
Figure 2.6 E_{HOMO} and E_{LUMO} as a function of dihedral angle between thiophene and **TD-P-TH-OMe** calculated by B3LYP/6-31G*……..…… 51
Figure 2.7 Orbital diagrams of HOMO and LUMO: (a) **P-TH-OCH$_3$**, (b) **TD-P-TH-OCH$_3$**, (c) **BP-TH-OCH$_3$**, and (d) **TD-BP-TH-OCH$_3$**……..…… 52
Figure 2.8 Energy-minimized structures of (a) **TD-P-TH-Me** and (b) **TD-P-MeTH-Me**……..….. 53
Figure 2.9 Optical micrographs of cast films: (a) **P-TH-OC10** (8 mg / mL $CHCl_3$), (b) **P-TH-C10** (15.3 mg / mL TCE), (c) **BP-TH-OC16** (4mg / mL $CHCl_3$), (d) **TD-P-TH-C10** (cross-polarized) (7 mg / mL $CHCl_3$), (e) **TD-P-diTH-C10** (cross polarized) (10^{-5}M $CHCl_3$) and (f) **TD-BP-TH-OC16** (2 mg / mL hot $CHCl_3$, cooled to RT, fibrous precipitate). Scale bar: 10 µm……...… 54
Figure 2.10 TEM images of cast films: (a, b) **BP-TH-OC16** (5.5 mg / mL hot $CHCl_3$, cooled to RT until precipitates formed) and (c, d, e) **TD-BP-TH-OC16** (0.7 mg / mL $CHCl_3$, and then 5mL MeOH slowly added. Left overnight. Purple precipitates), (f) **TD-BP-TH-OC16** (2 mg / mL hot $CHCl_3$, cooled to RT, partial gel)…….....56
Figure 2.11 UV-Vis absorption spectra of (a) **P-TH-OC10**, (b) **P-TH-C10**, (c) **BP-TH-OC16**, and (d) **TD-BP-TH-OC16** in $CHCl_3$ (solid line) and cast film (dotted line)……..….. 57

LIST OF SCHEMES

Scheme 1.1 Synthetic route to extended Phenazine-Acenes (system I)…….. 9

Scheme 1.2 Sonogashira cross-coupling of **PA-BTD-Br**……10

Scheme 2.1 (a) Synthetic routes to the target **PA-TH** molecules……....38

Scheme 2.1 (b) Synthetic routes to the target **PA-TH** molecules……..…..39

Scheme 2.1 (c) Synthetic routes to the target **PA-TH** molecules……...….40

CHAPTER 1

CONTROL OF E_{LUMO} BY EXTENSION OF THE PYRAZINE-ACENE π-CORE

1.1 Introduction

Control of electronic properties in organic semiconductor materials is essential for electro-optical applications such as field-effect transistors[1], light-emitting diodes[2], and photovoltaic devices[3-5]. Tunability of LUMO (E_{LUMO}) and HOMO (E_{HOMO}) energy levels is an important ingredient in the molecular design process as each application has various electronic requirements. The primary focus of this chapter is specific control of E_{LUMO} to create new electron deficient, n-type materials.[6,8,13,14,15,17,19,22,27]

N-Heteroacenes (aza-acenes) such as pyridine, pyrazine, and triazole have been particularly useful electron-deficient π-platforms.[6-15] In an effort to further increase the electron affinity (lowering of E_{LUMO}) of N-heteroacene containing materials, various approaches have been utilized. The synthetically simplest approach involves the introduction of electron-withdrawing peripheral substituents such as C≡N[6,16-22], NO_2[23], or halogens[24-31]. While this method effectively and conveniently lowers E_{LUMO}, additional structural functionalization is not feasible as the sites for modification become limited.

An alternative approach which provides greater flexibility in structural modification, although synthetically more challenging, involves extending the π-core by fusing additional contiguous electron-deficient N-heteroacene (or azaacene) moieties (π-extender henceforth). In this approach, it is important to place the π-extenders in an appropriate molecular location to maximize the E_{LUMO} lowering effect. For example, N-heteroacene units can be contiguously[7] or noncontiguously[8] incorporated within a molecular π-framework which can result in different E_{LUMO} lowering effects per pyrazine

unit. For system I, our goal is to explore the effect of π-extenders when they are fused with the pyrazine-acene (**PA**) (**Base PA** in Figure 1.1). More specifically, the π-extenders are fused directly to pyrazine in **Base PA** to maintain continuity. It is also our objective to find more effective E_{LUMO} lowering π-extenders which can replace the synthetically challenging repetitive addition of pyrazine units.

The π-extenders are chosen to investigate the effect of (i) the number of electron-deficient C=N functions, (ii) C=N function in a fused aromatic moiety in comparison to peripheral C≡N substituents, and (iii) benzothiadiazole (**BTD**)[32-37] in comparison to pyridine or pyrazine.

Having previously achieved exceptionally high correlation between computationally generated gap energies and those obtained experimentally[24], a significant aspect of this work involves the computational evaluation of the electronic properties associated with these π-extenders. Calculated energies are directly compared with all available experimental data. We have also added calculated energy data for molecules that we were not synthetically capable of generating in the laboratory. These additional systems help provide the most complete analysis of the π-extenders.

Furthermore, the self-assembly of synthesized compounds was studied using a variety of methods. The intent of each assembly method is to produce one-dimensional (1D) structures.[38-41] The efficient charge transport[42-44] has been attributed with the formation of 1D structures.

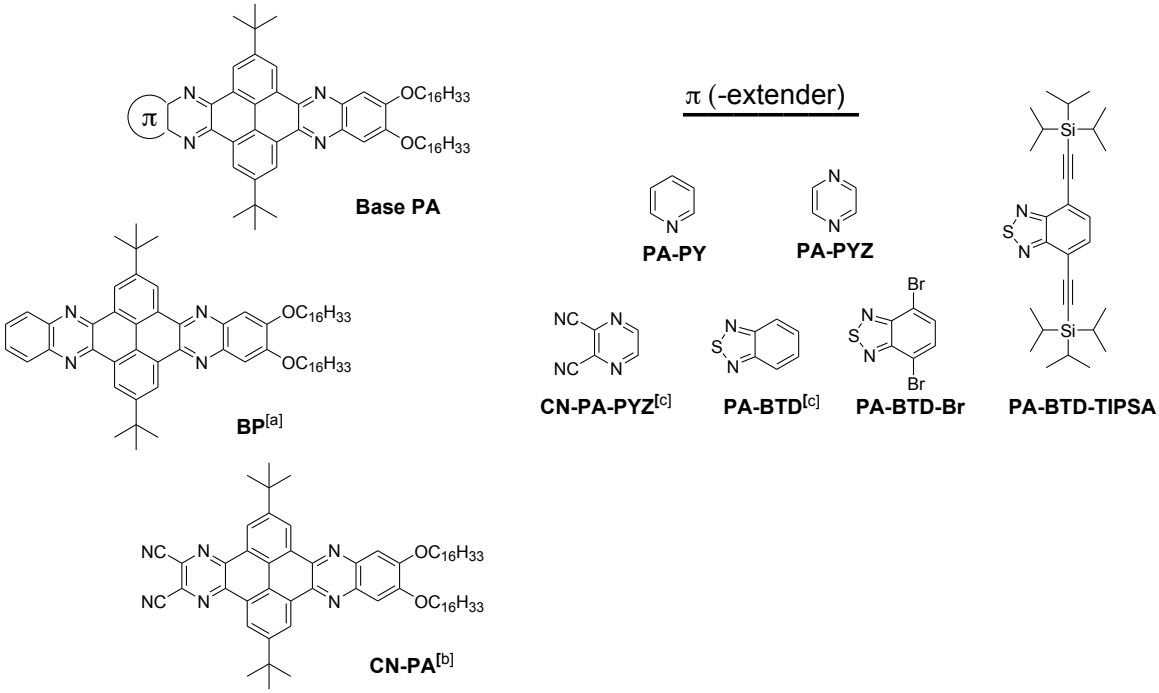

Figure 1.1. Pyrazine-acenes with π-extenders (system I). [a] Bisphenazine (**BP**)[23] [b]reference **PA** with peripheral cyano substituent. [c]synthetically unavailable and only presented with theoretical data.

1.2 Experiments

1.2.1 Instrumentation

Nuclear magnetic resonance (NMR) spectra were obtained with a Varian Gemini 400 MHz NMR spectrometer at room temperature. Deuterated chloroform ($CDCl_3$) containing tetramethylsilane (TMS) as an internal reference was used as the solvent for both ^{1}H NMR and ^{13}C NMR. Elemental Analysis was carried out by Atlantic Microlab, inc. Mass spectra were collected at the University of Illinois, Chicago. Optical properties of the molecules were obtained with Shimadzu UV-2600 UV-visible spectrophotometer and Horiba Fluorimeter using a xenon lamp excitation source for absorption and fluorescence emission, respectively. Electrochemistry measurements were performed using cyclic voltammetry (CV) on a CH instrument 660D with a three electrode

configuration, with a cell equipped with a platinum plate as the counter electrode, a platinum disc as the working electrode (2 mm diameter), and a non aqueous Ag/Ag^+electrode (Ag in 10 mM $AgNO_3$ solution in anhydrous acetonitrile) as the reference electrode. CV measurements for all compounds were recorded in a methylene chloride solution containing 0.1 M tetrabutylammonium hexafluorophosphate ($TBAPF_6$) as the supporting electrolyte. All solutions were purged with Ar for 20 - 30 min before each experiment, and a positive pressure of Ar was maintained over the sample solution during the experiments. The scan rate was ν = 100 mV/s for all experiments. All potentials are reported versus the ferrocene/ferrocenium (Fc/Fc^+) redox couple which was used as an internal standard. AFM was performed using non-contact AFM mode on a Park XE-70 in-air SPM system, using a NCHR cantilever.

1.2.2 Synthetic Procedures

All chemicals were purchased from commericial sources and used as received without further purification. The synthetic route to the title compounds can be seen in Scheme 1.1. The diketophenazine intermediate[45], and 4,7-Dibromo-benzo[1,2,5]thiadiazole-5,6-diamine[46] were prepared according to previously published procedures.

CN-PA To a round bottom flask containing 0.216 mmol of diketophenazine, acetic acid (10 mL) was added. Lastly, 0.259 mmol of maleonitrile was added to the flask. The resulting solution was stirred, under a nitrogen atmosphere, at 110°C for 12 hours. An additional 0.259 mmol of maleonitrile was added to the reaction flask, and stirring continued at 110°C for an additional 12 hours. Crude product was obtained by extracting into methylene chloride and washing with $NaHCO_3$ and water then dried over

sodium sulfate The product was purified by silica gel column chromatography (30 % methylene chloride in hexane) providing a yield of 56 % ^{1}H NMR (400 MHz, $CDCl_3$, ppm): δ 9.65 (2H, d, *J*=2.0 Hz), 9.25 (2H, d, *J*=1.8 Hz), 7.48 (2H, s), 4.31 (4H, t, *J*=6.6 Hz), 2.04 (4H, m), 1.72 (18H, s), 1.58 (4H, m), 1.45 (4H, m), 1.26 (44H, s), 0.88 (6H, t, *J*=6.8 Hz); ^{13}C NMR (100 MHz, $CDCl_3$, ppm): δ 153.60, 151.18, 143.27, 139.89, 138.90, 129.85, 129.39, 125.89, 125.64, 125.07, 123.92, 114.15, 106.56, 69.30, 35.91, 31.94, 31.83, 29.78, 29.76, 29.71, 29.70, 29.50, 29.39, 29.01, 26.15, 22.70, 14.13. $[M^{+}H]^{+}$:Calcd 999.7; Found 999.7.

PA-PY To a round bottom flask containing 0.216 mmol of diketophenazine, cholorform (8.4 mL) and acetic acid (2.7 mL) were added. 0.216 mmol of 2,3-diaminopyridine was added to the flask lastly. The resulting solution was stirred, under a nitrogen atmosphere, at 80°C for 14 hours. Precipitates obtained after cooling the reaction solution were filtered and rinsed with $NaHCO_3$, H_2O and methanol. The product was purified by silica gel column chromatography (60 % methylene chloride in hexane) providing a yield of 85 % ^{1}H NMR (400 MHz, $CDCl_3$, ppm): δ 9.90 (1H, d, J=2.2 Hz), 9.79 (2H, overlapping doublets), 9.72 (1H, d, *J*=2.2 Hz), 9.34 (1H, dd, *J*=4.0, 1.9), 8.80 (1H, dd, *J*=8.4, 2.0 Hz), 7.85 (1H, dd, *J*=8.4, 3.9 Hz), 7.62 (2H, d, *J*=1.8 Hz), 4.33 (4H, t, *J*=6.7 Hz), 2.01 (4H, m), 1.74 (18H, s), 2.02 (4H, m), 1.61 (4H, m), 1.42 (4H, m), 1.26 (44H, s), 0.88 (6H, t, *J*=6.9 Hz); ^{13}C NMR (100 MHz, $CDCl_3$, ppm): δ 153.32, 150.92, 143.01, 139.58, 138.51, 129.72, 129.11, 125.71, 125.39, 124.71, 123.14, 114.14, 106.32, 69.21, 35.86, 31.96, 31.84, 29.80, 29.77, 29.74, 29.71, 29.53, 29.40, 29.02, 26.15, 22.72, 14.14. $[M^{+}H]^{+}$: Calcd 1000.7 Found 1000.7

PA-PYZ To a round bottom flask containing 0.755 mmol of diketophenazine, chloroform (25 mL) and acetic acid (25 mL) were added. 0.755 mmol of 2,3-diaminopyrazine was added to the flask lastly. The resulting solution was stirred, under a nitrogen atmosphere, at 70°C for 7 days. Precipitates obtained after cooling the reaction solution were filtered and rinsed with $NaHCO_3$, H_2O and methanol. The product was purified by silica gel column chromatography (1 % ethyl acetate in methylene Chloride) providing a yield of 18 % ^{1}H NMR (400 MHz, $CDCl_3$, ppm): δ 9.84 (4H), 9.30 (2H, s), 7.27 (2H, s), 4.34 (4H, t, *J*=6.6 Hz), 2.03 (4H, m), 1.67 (18H, s), 1.61 (4H, m), 1.46 (4H, m) 1.26 (44H, s), 0.88 (6H,t, *J*=7.0 Hz); ^{13}C NMR (100 MHz, $CDCl_3$, ppm): δ 153.64, 151.23, 148.52, 147.49, 145.10, 140.16, 139.99, 129.97, 128.14, 125.78, 125.45, 106.88, 69.31, 35.98, 31.94, 31.83, 29.75, 29.68, 29.45, 29.38, 28.95, 26.13, 22.70, 14.12. (1 aromatic peak and 7 alkyl peaks not seen due to overlapping signals) $[M^+H]^+$: Calcd 1001.5 Found 1001.8

PA-BTD-Br To a round bottom flask containing 0.329 mmol of diketophenazine, acetic acid (16 mL) was added. 0.494 mmol of 5,6-diamino-4,7-dibromo-2,1,3-benzothiadiazole was added to the flask lastly. The resulting solution was stirred, under a nitrogen atmosphere, at 90°C for 18 hours. Precipitates obtained after cooling the reaction solution were filtered and rinsed with $NaHCO_3$, H_2O and methanol. The product was purified by silica gel column chromatography (50 % methylene chloride in hexane) providing a yield of 57 % ^{1}H NMR (400 MHz, $CDCl_3$, ppm): δ 9.64 (4H, s), 7.44 (2H, s), 4.19 (4H, t), 2.00 (4H, m), 1.61 (4H, m), 1.47 (4H, m), 1.27 (44H,s), 0.88 (6H, t, *J*=6.4 Hz); ^{13}C NMR was unable to be preformed due to poor solubility at concentrations required for ^{13}C NMR measurements. $[M^+H]^+$: Calcd 1213.4 Found 1213.4

PA-BTD-TIPSA To a round bottom flask containing 0.247 mmol EBP-BTD-Br with 8mol% $PdCl_2(PPh_3)_2$, 45 mL THF and 15 mL triethylamine were added (both degassed with Argon prior to use). 0.741 mmol of (triisopropylsilyl)acetylene was added via syringe and 8mol% CuI was added lastly. The reaction mixture stirred under nitrogen for 2.5 hours at 65°C. The resulting mixture was filtered over a silica pad and further purified by column chromatography (30% methylene chloride/hexane) and recrystallization from hexane and methanol to provide a yield of 19 %. ^{1}H NMR (400MHz, $CDCl_3$, ppm) 9.83 (2H, d, *J*=2.0 Hz), 9.76 (2H, d, *J*= 2.0 Hz), 7.63 (2H, s), 4.34 (4H, t, *J*= 6.6Hz), 2.03 (4H, m), 1.73 (18H, s), 1.61 (4H, m), 1.36-1.26 (90H, overlapping peaks), 0.88 (6H, t, *J*=6.8 Hz) ^{13}C NMR was unable to be preformed due to poor solubility at concentrations required for ^{13}C NMR measurements. . $[M^+H]^+$: Calcd 1417.0 Found 1418.1

1.2.3 Organogelation

A suspension was created in a 4 mL screw cap vial with a weighed amount of each compound, and dissolved by heating in an organic solvent. The homogenous solution was allowed to cool to room temperature. Gelation was considered successful if no flow was observed upon inversion of the vial.[47]

1.2.4 Gelling Temperature (T_{gel})

T_{gel} was determined by forming a gel and placing the vial inverted into a temperature regulated water bath. The temperature of the water was monitored while being slowly increased. The temperature at which the gel fell from the bottom of the vial was recorded as T_{gel} for that compound.[47]

1.2.5 Phase Transfer Assembly[41,43]

A binary solvent system with methylene chloride and methanol was used for phase transfer (PT) assembly. All solvents were filtered through a 0.2 μm PTFE filter before each experiment. Each compound was dissolved in methylene chloride and filtered into a clean 20 mL screw cap vial. Filtered methanol was slowly added so that two phases could be maintained. The mixture was left undisturbed overnight to let the two phases mix slowly. A variety of concentrations were tested as well as various volume ratios of methylene chloride/methanol.

1.3 Results and Discussion

1.3.1 Synthesis

The title compounds were prepared from a condensation reaction between the diketophenazine intermediate and various diamino compounds. (Scheme 1.1) The yield for the condensation reaction varied from 18% to 85% depending upon the type of diamines.

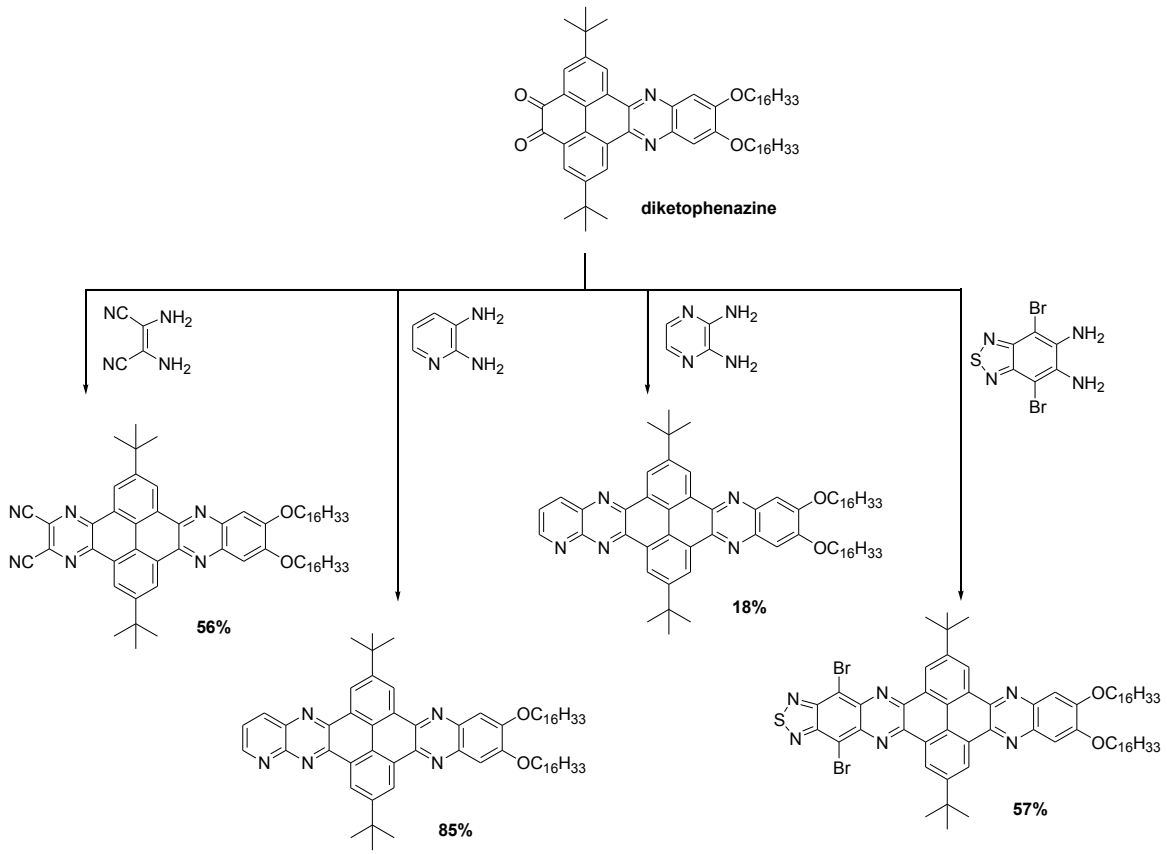

Scheme 1.1. Synthetic route to extended Phenazine-Acenes (system I).

We note that the reactivity of heteroaromatic diamines, i.e., 2,3-diaminopyridine, 2,3-diaminopyrazine, and 5,6-diamino-2,3-dicyanopyrazine, could be correlated to the electron-withdrawing nature of heteroaromatic rings. When the heteroaromatic ring contained one electron-withdrawing imine N (pyridine), the reactivity of dimine was not influenced when compared to *o*-diaminobenzene[23], giving 85% yield for the condensation reaction which produced **PA-PY**. In the case of 2,3-diaminopyrazine which contained two imine N, the reactivity of diamine dropped significantly producing **PA-PYZ** with a low yield of 18%. However, our attempt to synthesize **CN-PA-PYZ** was unsuccessful. Although there is a report on the preparation of a dicyanopyrazinopyrazine,[6,8] extending bisphenazine with dicyanopyrazine was not possible. Nevertheless, this result is

consistent with the trend of the reactivity of diamine we observed. Presumably, the electron-withdrawing C≡N substituents on the pyrazine ring further decreased the reactivity of diamine. However, this trend of the diamine reactivity may not be applicable to 4,7-dibromo-benzo[1,2,5]thiadiazole-5,6-diamine or diaminomalenonitrile, since **PA-BTD-Br** and **CN-PA** were obtained in moderate yields of 57% and 56%, respectively, in spite of the electron-withdrawing nature of the substituent, i.e., dibromobenzothiadiazole and cyano groups.

The intermediate necessary for the synthesis of **PA-BTD** was not able to be made due to uncontrollable nitration in the absence of bromine on the aromatic ring.[48] The Br substituents in **PA-BTD-Br** provided us an opportunity to further introduce substituents using a Pd-catalyzed C-C coupling reaction. We conducted Sonogashira coupling of **PA-BTD-Br** with (triisopropylsilyl)acetylene to give **PA-BTD-TIPSA** at 18% yield. (Scheme 1.2) This low yield could be attributed to instability of **PA-BTD-Br** under the reaction conditions as monitored by TLC. Since we did not observe unreacted **PA-BTD-Br**, the reactant may not be stable under the reaction conditions. Reactions using **PA-BTD-TIPSA** proved unattainable, as removal of the protective triisopropylsilyl protecting group resulted in an unknown product that could not be isolated.

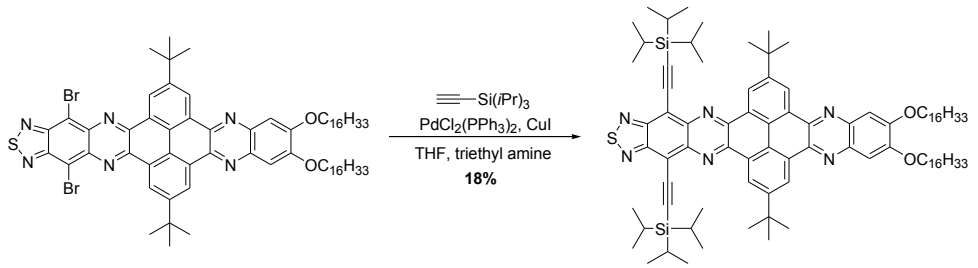

Scheme 1.2. Sonogashira cross-coupling of **PA-BTD-Br**

The structures and purity of the title compounds were confirmed by ^{1}H NMR, ^{13}C NMR, and mass spectrometry. Due to solubility issues with **PA-BTD-Br** and **PA-BTD-TIPSA**, reasonable 13C NMR spectra were not obtained.^{13}C was not performed.

1.3.2 Physical Properties

1.3.2.1 Optical Properties

The UV-Visible absorption spectra for the title compounds are shown in figure 2. To ensure that the absorptions are due to intrinsic properties of the molecules rather than aggregation, a concentration study was performed. All compounds followed Beer's law in $CHCl_3$ solutions in the concentration range used (10^{-6} M to 5 x 10^{-6} M). From the Beer's plot, the molar absorptivity values were calculated (Table 1.1).

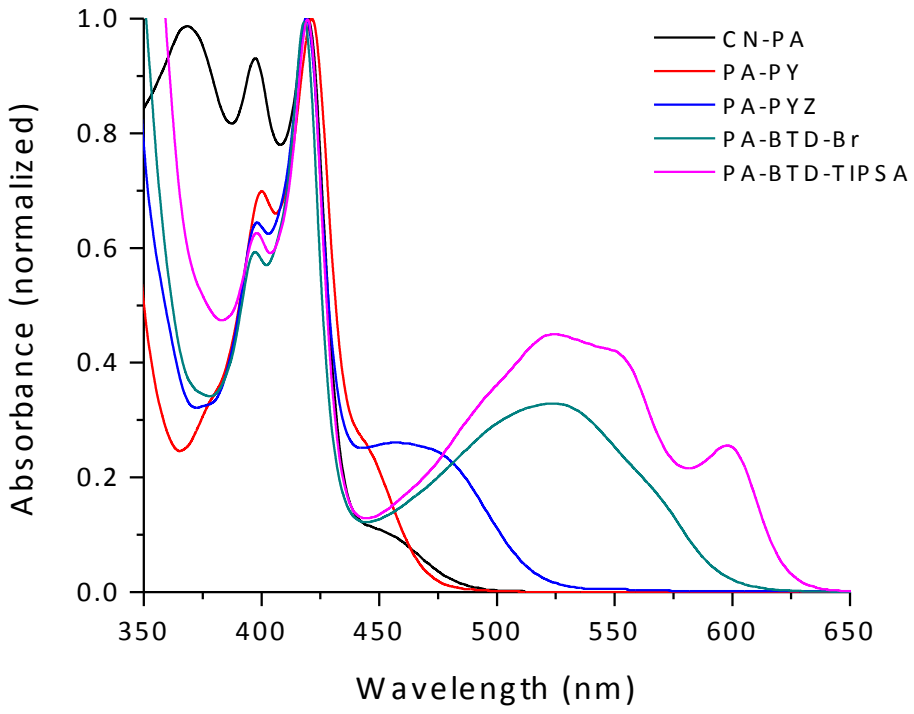

Figure 1.2. UV-Vis spectra of system I.

All compounds showed λ_{max} at ca. 420 nm and the molar absorptivities at λ_{max} were in the range of ca. 40,000–80,000 M^{-1} cm^{-1}. In addition to λ_{max} at ca. 420 nm, **CN-**

PA and **PA-PY** showed small shoulders at ca. 450 nm and ca. 446 nm, respectively. A more pronounced shoulder was observed for **PA-PYZ** at ca. 460 nm. In the case of **PA-BTD-Br** and **PA-BTD-TIPSA**, additional peaks at 525 nm and 598 nm, respectively, were observed.

Table 1.1. Molar absorbtivity and Fluorescence quantum efficiency of System I.

	ε (at 420 nm, $M^{-1}cm^{-1}$)	**Φ_F[a]**
CN-PA	4.3×10^4	0.16
PA-PY	8.3×10^4	0.11
PA-PYZ	5.2×10^4	0.2
PA-BTD-Br	7.0×10^4	NA[b]
PA-BTD-TIPSA	5.9×10^4	0.03

[a] Measured with diphenyl anthracene as a standard (Φ_F=0.90), excitation at 360 nm.
[b] Unable to determine accurate efficiency ($\Phi_F < 0.05$).

By taking the tangent of the absorption edge, the optical gap (E_{gap}) was estimated, and these values are summarized in Table 2. From **PA-PY** to **PA-BTD-TIPSA**, a significant compression of E_{gap} by 0.78 eV was achieved.

The emission properties were also characterized in $CHCl_3$. The fluorescence maxima of the compounds followed the trend of E_{gap} calculated from UV-Vis absorption spectroscopy, with **PA-PY** showing the shortest and **PA-BTD-TIPSA** the longest wavelength, respectively (Fig. 2). The λ_{em} values for **PA-PY**, **CN-PA**, and **PA-PYZ** were found to be 505 nm, 534 nm, and 555 nm, respectively when excited at λ_{max}. The fluorescence quantum efficiencies for **CN-PA** and **PA-PY** measured with diphenylanthracene (Φ_F = 90%) as the reference were 18 and 12%, respectively. In the case of **PA-PYZ**, the Φ_F was significantly reduced to 3%. The λ_{em} for **PA-BTD-Br** were red-shifted to 614 nm with a negligible Φ_F. **PA-BTD-TIPSA** showed the most red-

shifted λ_{em} at 616 nm with a small shoulder at ca. 665 nm. The Φ_F value for **PA-BTD-TIPSA** was found to be 3%.

1.3.2.2 Electrochemical Properties

Electrochemical properties of the title compounds were studied using cyclic voltammetry (CV) in CH_2Cl_2 with $TBAPF_6$ (0.1 M) and $Ag/AgNO_3$ in CH_3CN as the supporting electrolyte and reference electrode solution, respectively. Ferrocene was added as an internal reference (6-10 drops of an 8 mM solution in methylene choloride was added to each solution). As shown in figure 3, all compounds displayed quasi-reversible reduction waves, where i_{pc}/i_{pa} is greater than 1, suggesting that the first reduction is energetically favored over the subsequent oxidation. In the case of **CN-PA**, **PA-PY**, and **PA-PYZ**, one reduction potential was observed whereas **PA-BTD-Br** and **PA-BTD-TIPSA** showed two reduction waves within the potential window characterized.

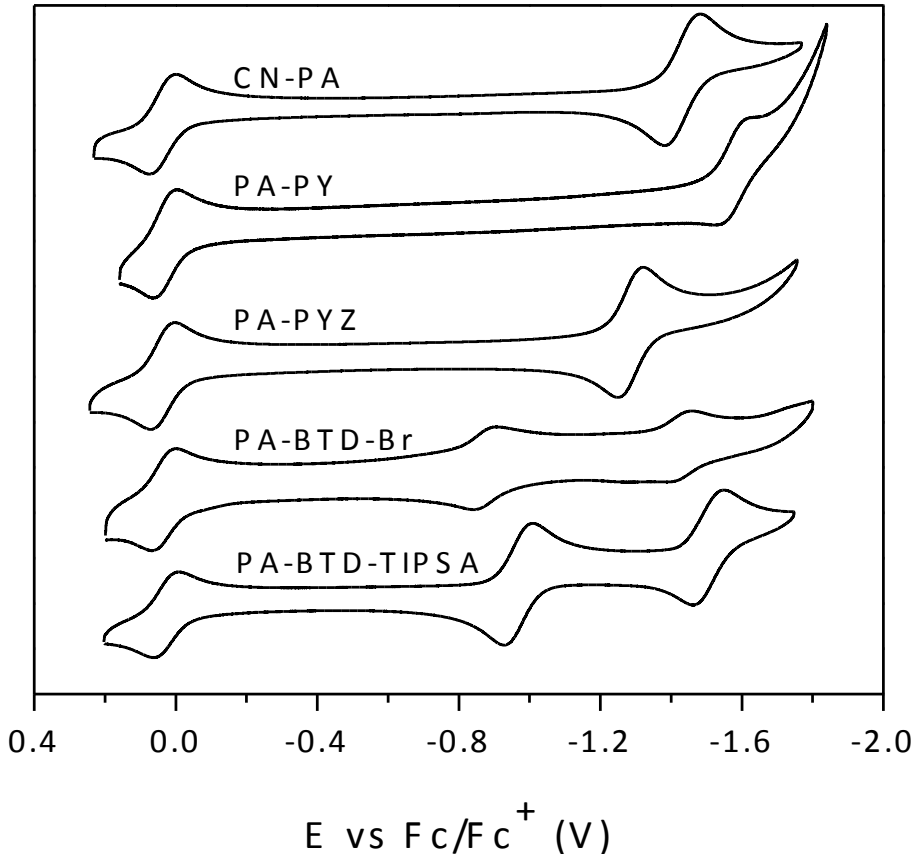

Figure 1.3. Cyclic voltammograms of System I.

Using the onset of the first reduction potential, E_{LUMO} was calculated based on the ferrocene's oxidation potential of -4.8 eV with respect to the vacuum level. When compared to **BP**[23], **CN-PA** showed ΔE^{EXP}_{LUMO}(=E^{EXP}_{LUMO} of **BP** (-3.12 eV) - E_{LUMO} of compounds in this work) of 0.31 eV. In the case of **PA-PY**, $\Delta E^{EXP}_{LUMO}$was found to be 0.15 eV, indicating that the pyridine π-extender (with one imine nitrogen) was less effective than two C≡N groups for lowering E_{LUMO}. However, the pyrazine π-extender (with two imine nitrogens) in **PA-PYZ** was more effective in lowering E_{LUMO} than two C≡N groups, showing a ΔE^{EXP}_{LUMO} of 0.42 eV. An interesting aspect is that $\Delta E^{EXP}_{LUMO}$of **PA-PYZ** was greater than **CN-PA** $\Delta E^{EXP}_{LUMO}$of **PA-PY**. Indeed, this result was in good qualitative

agreement with the significantly reduced reactivity of 2,3-diaminopyrazine compared to that of 2,3-diaminopyridine as described in the synthesis section.

The most significant LUMO lowering was observed for **PA-BTD-Br** with E_{LUMO} of -3.95 eV (ΔE_{LUMO}^{EXP} = 0.83 eV). When Br was replaced by TIPSA (**PA-BTD-TIPSA**), E_{LUMO} was only slightly increased to -3.87 eV. This result demonstrates that a proper choice of π-extender can impact E_{LUMO} lowering much more than simply increasing the number of imine N's.

1.3.3 Theoretical Evaluation

A computational investigation into the electronic properties of all structurally modified systems was carried out and correlated with available experimental data. Initially, geometries were optimized at the B3LYP/6-31G* level of theory.[49] Next, single point calculations (B3LYP/6-31+G*//B3LYP/6-31G*) were run, adding diffuse character to the heavy atoms (all atoms except hydrogen) in our systems.

Results from these calculations are presented in Table 2. Finally, using the same, initially optimized geometries, time-dependent (TD)-DFT was employed to determine the vertical S_0 - S_1 electronic transition ($S_1^{Vertical}$). These calculations agree with the experimental trend. All energies were calculated using the Gaussian electronic structure suite programs.[50] We note that a strong correlation exists between all theoretical methods employed and experimental E_{LUMO} and E_{gap} energies.

The experimental E_{HOMO} value was calculated by subtracting E_{LUMO} (from CV) from E_{gap} (from UV-Vis), as we were unable to obtain E_{HOMO} from CV experiments due to oxidation difficulties associated with these compounds. Both theoretical and

experimental electronic properties are summarized in Table 2 and graphically presented in Figure 1.4 for easier visualization of relative E_{HOMO} and E_{LUMO} values.

Table 1.2. Summary of system I electronic properties.

	E_{LUMO}[a] [eV]	E_{HOMO}[b] [eV]	E_{gap}[c] [eV]	$\mathbf{E_{LUMO}^{THEO}}$[a] [eV]	$\mathbf{E_{HOMO}^{THEO}}$[e] [eV]	$\mathbf{E_{gap}^{THEO}}$[f] [eV]	$\mathbf{S_1^{vertical}}$[g] [eV]
CN-PA	-3.43	-6.01	2.58	-3.05	-6.19	3.14	2.78
BP[d]	-3.12	-5.86	2.74	-2.43	-5.76	3.33	2.98
PA-PY	-3.27	-6.04	2.77	-2.66	-5.83	3.17	2.84
PA-PYZ	-3.54	-5.93	2.39	-2.98	-5.91	2.93	2.63
CN-PA-PYZ	NA	NA	NA	-3.89	-6.27	2.38	2.10
PA-BTD	NA	NA	NA	-3.36	-5.95	2.59	2.30
PA-BTD-Br	-3.95	-6.11	2.16	-3.62	-6.02	2.40	2.12
PA-BTD-TIPSA	-3.87	-5.86	1.99	-3.53	-5.67	2.14	1.90

[a] from cyclic voltammetry [b] $E_{HOMO}=E_{LUMO}-E_{gap}^{optical}$. [c] from UV Vis [d] Reference 23 [e] B3LYP/6-31+G* [f] E_{LUMO}^{THEO}- E_{HOMO}^{THEO}. [g] $S_0 \rightarrow S_1$ vertical transition. The transitions are all one electron with the highest HOMO-LUMO contribution, NA not available.

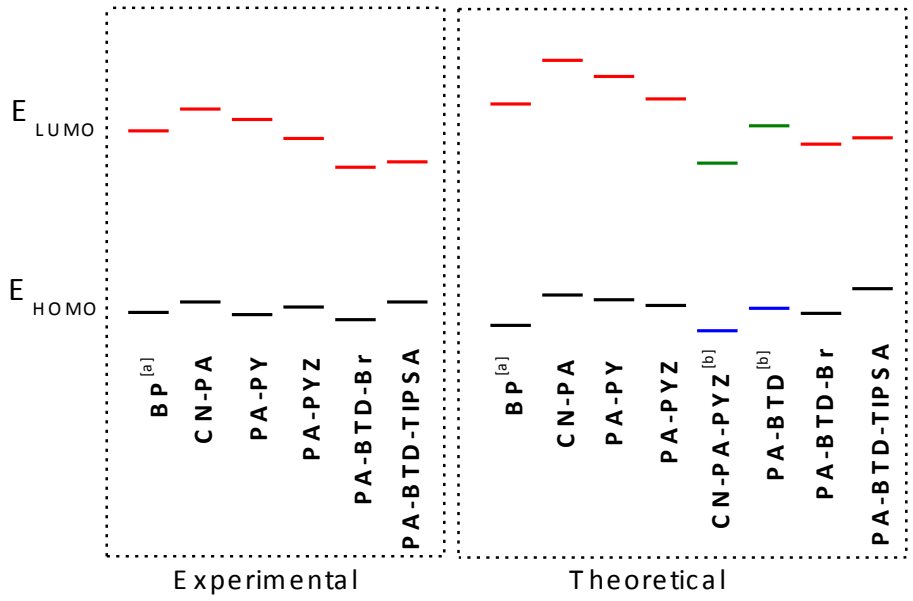

Figure 1.4. Graphical representation of electronic properties. [a]reference 23,[b] Synthetically unavailable. Numerical values are provided in Table 1.2.

In addition, a linear regression analysis was used to compare theoretical and experimental E_{LUMO}. As shown in figure 1.5, impressive correlation between theoretical and experimental E_{LUMO} was observed, yielding an r^2 value of 0.96626. This high level of correlation is consistent with our past theoretical and experimental collaboration on structurally related systems and provides the confidence in our subsequent comparative interpretation.

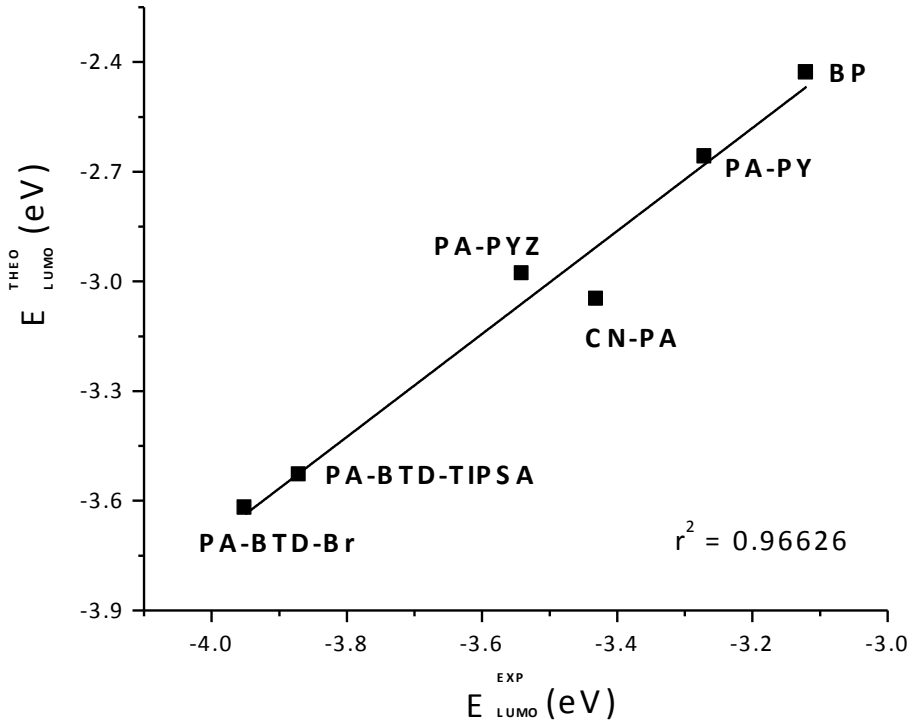

Figure 1.5. Correlation between E_{LUMO} obtained experimentally and theoretically.

We note that E_{LUMO} is greatly impacted by the types of π-extenders (i.e., pyridine, pyrazine, benzothiadiazole, etc.), while E_{HOMO} is not significantly affected. For example, when the number of imine nitrogens in the π-extender increased from one (**PA-PY**) to two (**PA-PYZ**), E_{LUMO} decreased by ca. 0.3 eV. The E_{HOMO} for this system increased only by ca. 0.1 eV. These results were found both theoretically and experimentally. Significant insight into these findings can be achieved by observing the localization of the HOMO and LUMO molecular orbitals, which are situated on different areas of the molecular framework (Figure 1.6). These molecular orbital pictures are useful in gaining understanding into the electronic properties of our system, and the subsequent changes that take place upon structural modification. The orbital diagrams of **PA-PY** are not

presented as they exhibit the same trend as **PA-PYZ**. In the case of **PA-PY**, **PA-PYZ**, and **PA-BTD-Br**, the more electron-rich part of the compound, i.e., phenazine with hexadecyloxy substituents, showed significant HOMO orbital coefficients. Meanwhile, the LUMO orbital coefficients for these three compounds showed increased values in the π-extender section. As a result, E_{LUMO} was influenced more significantly by the electronic deficiency of the p-extender. The same trend was observed for **CN-PA** in which the more electron-deficient component is the C≡N peripheral substituent, rather than the π-extender. It should be noted that theory estimated more E_{HOMO} lowering for C≡N substituents (**PA-CN** and **CN-PA-PYZ**) than for π-extenders, although the HOMO orbital is localized on the phenazine with hexadecyloxy substituents. All molecular orbitals were generated using the Spartan electronic structure program.[51] Interestingly, we found a similar trend with benzothiadiazole (BTD) containing compounds. When **PA-BTD** (experimentally unavailable), **PA-BTD-Br**, and **PA-BTD-TIPSA** were compared, it was clear that the HOMO orbitals of **PA-BTD** and **PA-BTD-TIPSA** localized on the similar portion of the molecules, producing nearly equivalent E_{HOMO} values. However, the HOMO orbital of **PA-BTD-TIPSA** was heavily localized on the aryleneethynylene rather than the phenazine-hexadecyloxy part of the molecule. As mentioned earlier, HOMO orbital coefficients localize on the more electron rich part of the molecule. In the case of **PA-BTD-TIPSA**, the aryleneethynylene portion is presumed to be more electron rich than the phenazine-hexadecyloxy part due to the presence of the relatively electropositive Si. [55] As a result, we observed an increased E_{HOMO}^{THEO} of **PA-BTD-TIPSA** relative to **PA-BTD-Br** by 0.35 eV (0.25 eV experimentally). Additionally, it should be noted that E_{LUMO}^{THEO} was decreased by 0.26 eV when Br was introduced to BTD due to the

electronegative nature of the halogens. When Br was replaced by TIPSA on BTD, the E_{LUMO}^{THEO} decrease was 0.17 eV. This finding gives us the possibility of independently controlling not only E_{LUMO} but E_{HOMO} as well. Using the knowledge of where LUMO and HOMO orbitals are found on the PAs of system I allowed for the smart design of compounds presented in Chapter 2 (system II).

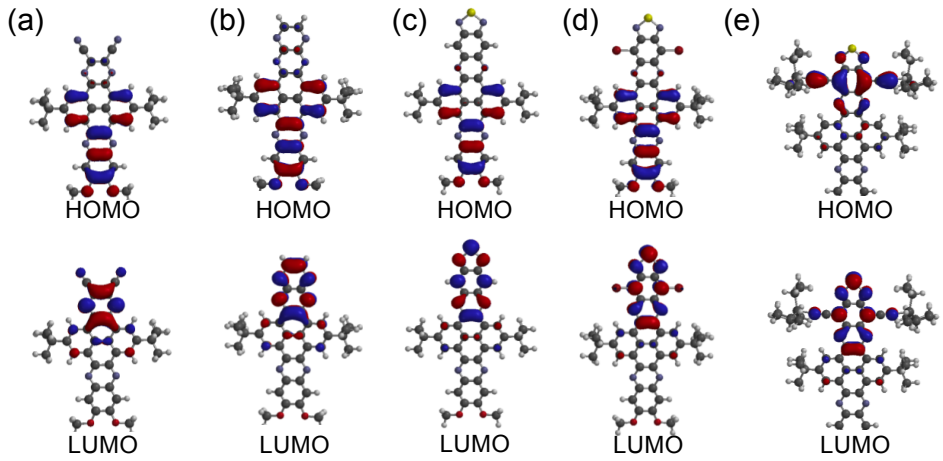

Figure 1.6. Molecular orbital diagrams of System I: (a) **CN-PA**, (b) **PA-PYZ**, (c**) PA-BTD**, (d) **PA-BTD-Br**, and (e) **PA-BTD-TIPSA**.

1.3.4 Assembly Properties

The 1D assembly of this series of compounds was first studied using organogelation[52-54] which is a facile and reproducible way of forming 1D fibers. In cases where we were not able to find a gelation solvent for a given compound, a phase transfer (PT) method was employed as an alternative way to induce 1D fibers.[43] The organogelation of each compound was tested using the inverse flow method[47] in various solvents at various concentrations in a 4 mL scintillation vial (15 mm diameter) and is summarized in Table 1.3.

Table 1.3. Gelation test of System I compounds.

Solvent	CN-BP	EBP-Py	EBP-PYZ	EBP-BTD-Br
Cyclohexane	S	Gel (10mM, 45 °C)	Gel (4mM, 37 °C)	NS
Hexane	S	ppt	ppt	NS
toluene	S	S	S	ppt
Ethyl acetate	ppt	ppt	ppt	ppt
THF	S	S	S	ppt
TCE	S	S	Gel (26mM, 34 °C)	ppt
DCE	S	ppt	ppt	ppt
CCl_4	S	S	S	ppt
MeOH	NS	NS	NS	NS
EtOH	NS	NS	NS	NS
Propanol	ppt	ppt	ppt	NS
CH_3CN	ppt	NS	NS	ppt
$CHCl_3$	S	S	S	PG
$CDCl_3$	S	S	S	PG

[a] Abbreviations: G, gel; PG, partial gel; ppt, precipitation upon cooling; S, soluble after cooling; NS, not soluble. Critical Gel Concentration (CGC) followed by T_{gel} is shown in parentheses.

Among all the compounds, only **PA-PY** and **PA-PYZ** were capable of forming organogels. **PA-PY** required a concentration of 10 mM in cyclohexane to form a gel with a T_{gel} of 45 °C, while a lower concentration in cyclohexane was necessary for **PA-PYZ** (4 mM, T_{gel} =37 °C). Furthermore, **PA-PYZ** also gelled in 1,1,1-trichloroethane at a

concentration of 26 mM (T_{gel} = 34 °C). Meanwhile, **CN-PA** did not form a gel in the solvents tested, however it was successfully assembled by the PT method using methylene chloride and methanol as a good and poor solvent, respectively. In the case of compound **PA-BTD-Br**, only a partial gel was obtained in $CHCl_3$ or $CDCl_3$.

The macroscale morphology of the self-assembled clusters was initially investigated using an optical microscope. As shown in Figure 1.7, straight 1D fibers were clearly observed for **CN-PA** which was assembled by the PT method. Xerogels of **PA-PY** and **PA-PYZ** (from cyclohexane gels) showed rather flexible fibers, while **PA-BTD-Br** (from partial gel in $CHCl_3$) showed straight fibers. All of the fibers had a thickness of roughly a few hundred nanometers.

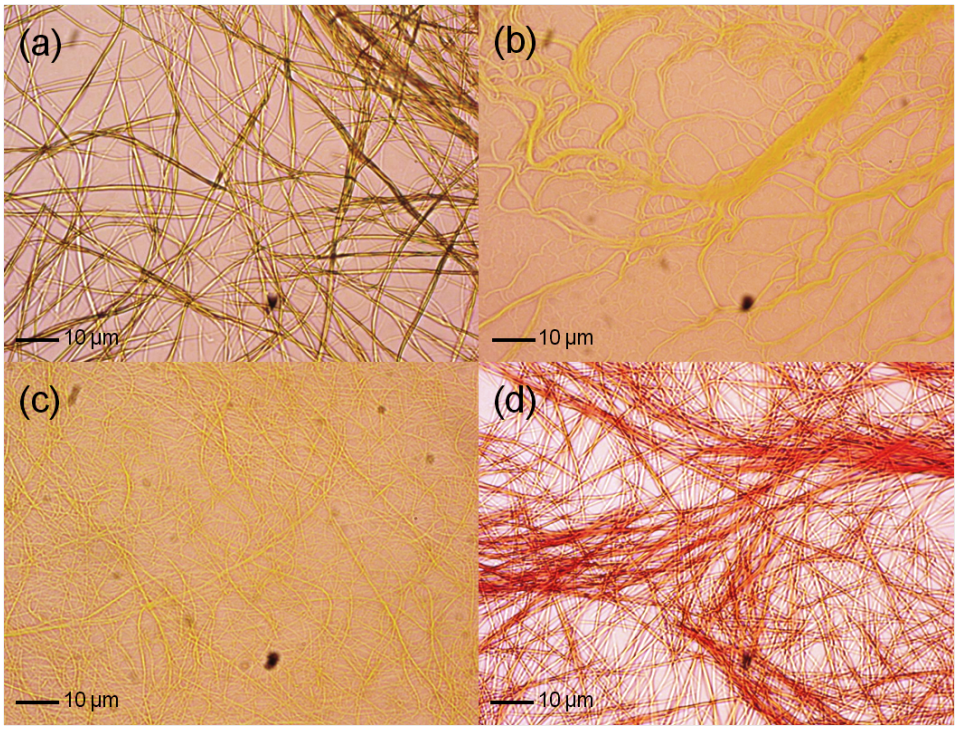

Figure 1.7. Polarized Optical Microscopy of (a) **CN-PA** from PT; (b) **PA-PY** (10 mM cyclohexane gel); (c) **PA-PYZ** (26 mM TCE gel); (d) **PA-BTD-Br** (4 mM $CHCl_3$ partial gel).

To investigate the microscale morphology, the assembled fibers were characterized by non-contact mode atomic force microscopy (NC-AFM). As shown in Figure 1.8, AFM images clearly illustrate the fiber morphology similar to the results obtained from the optical microscope characterization. The fibers of **CN-PA** formed from the PT assembly showed straight, rigid fibers with a width of ca. 1 μm (Figure 1.8a and e). Dried gels of **PA-PY** and **PA-PYZ** exhibited thinner fibers with widths of ca. 200 nm for **PA-PY** (Figure 1.8b and f) and ca. 300–400 nm for **PA-PYZ** (Figure 1.8c and g).

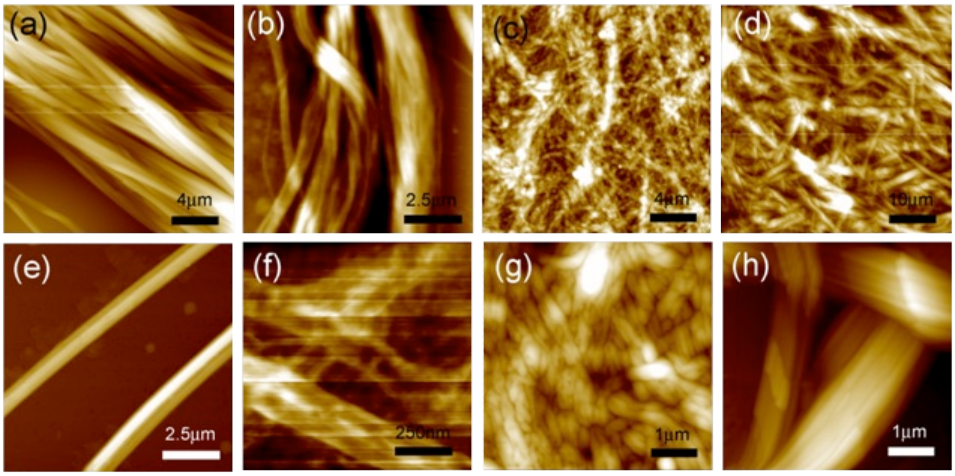

Figure 1.8 AFM images of (a and e) **CN-PA** assembled by the PT method (2 mL of 1 mM methylene chloride solution/2 mLMeOH); (b and f) cyclohexane gel of **PA-PY** (10 mM) dispersed in hexane; (c and g) xerogel from cyclohexane gel of **PA-PYZ** (4mM); (d and h) partial gel of **PA-BTD-Br** from $CHCl_3$ (4 mM). Image size: (a) 20 μm × 20 μm, (b) 10 μm ×10 μm, (c) 20 μm × 20 μm, (d) 50 μm × 50 μm, (e) 10 μm ×10 μm, (f) 1 μm ×1 μm, (g) 5 μm ×5 μm, and (h) 5 μm ×5 μm.

It should be noted that the fiber sample of **PA-PY** was prepared by dispersing a cyclohexane gel (10 mM) in hexane. This process was required because of the dense bundling of fibers, which hampered characterization of isolated fibers. The fibers of **PA-BTD-Br** from the partial gel were ca. 1–2 μm in width (Figure 1.8d and h). Interestingly,

despite the presence of the bulky triisopropylsilyl group, **PA-BTD-TIPSA** formed short needles rather than 1D fibers (not shown). Although we attempted to solve the structure by single crystal X-ray diffraction, we were able to obtain only a partial crystal structure in which π-cores were arranged in an antiparallel fashion (Figure 1.9).

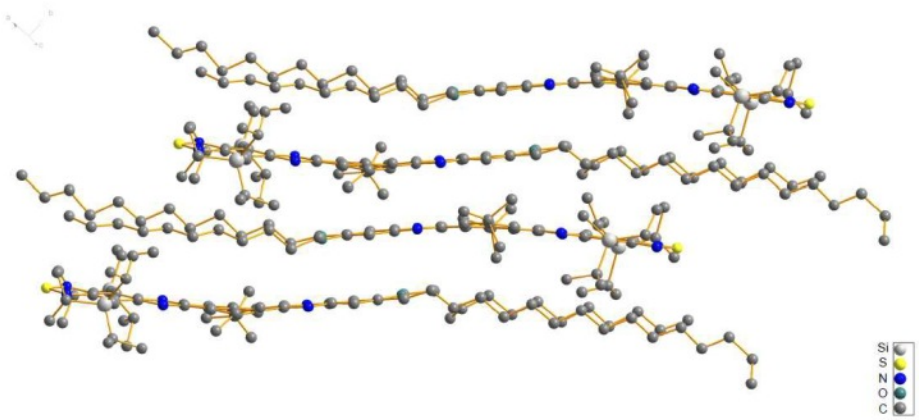

Figure 1.9 Partial crystal structure of **PA-BTD-TIPSA**.

The absorption behavior of the fibers were further characterized and compared with those in the solution state. Figure 1.9 shows the UV-Vis spectra of compounds **PA-PY** and **PA-PYZ**, respectively, as the gel and solution state in cyclohexane. Note that the dilute solutions of **PA-PY** and **PA-PYZ** in cyclohexane exhibited more structured absorption characteristics compared to those in $CHCl_3$. These solvent-dependent spectral differences were not caused by molecular aggregation. This hypothesis was verified by both concentration studies and variable temperature UV-Vis absorption spectroscopy. The concentration study in cyclohexane showed that the absorptions followed Beer's law. In addition, the absorption spectra at room temperature were identical to those at 60 °C. In both cases, spectra in the gel states showed clear redshifts in the absorption maxima compared to those in the solution state. The cyclohexane solution of **PA-PY** showed λ_{max}

at 418 nm and a shoulder at 441 nm. These peaks were red-shifted to 432 nm and 455 nm, respectively, in the gel state. A similar trend was observed from compound. The λ_{max} at 416 nm and the shoulder at 468 nm in the solution state red-shifted to 429 nm and 484 nm, respectively, in the gel state. These results strongly suggest that the fibrillation during the gelation process is driven by π–π interactions. Note that we were unable to obtain reasonable absorption spectra for the fibers from **CN-PA** and **PA-BTD-Br** because of their larger fiber size.

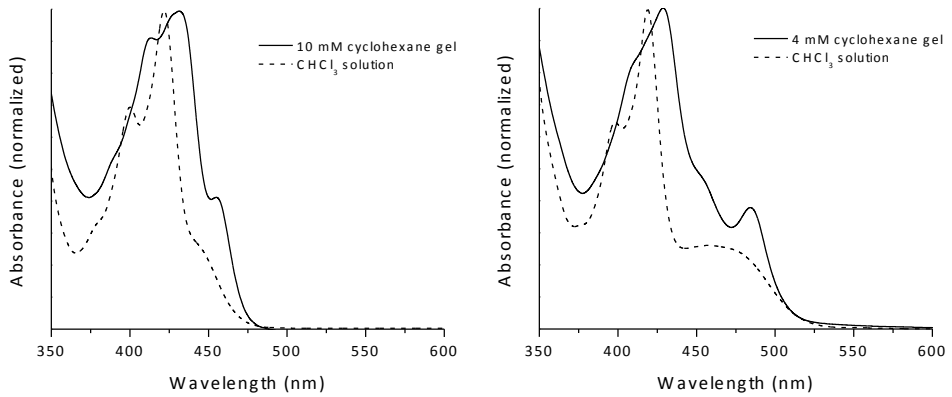

Figure 1.10. UV Vis spectra of (a) **PA-PY** and (b) **PA-PYZ** in the gel and solution state.

1.4 Conclusions

A series of pyrazine-acenes fused with electron-withdrawing π-extenders, including pyridine, pyrazine, and benzothiadiazole have been successfully synthesized and characterized. Electronic properties have been characterized using UV Vis spectroscopy and cyclic voltammetry which revealed that these π-extenders are effective in controlling E_{LUMO} specifically.

The comparison of **CN-PA** and **PA-PYZ** revealed that C=N function is slightly more effective in lowering E_{LUMO} than C≡N. From **PA-PY** to **PA-PYZ**, we found that E_{LUMO} was reduced by 0.27 eV, showing the effect of the increased number of C=N

functions. The most profound effect was seen when BTD was used as a π-extender. A decrease in E_{LUMO} of 0.83 eV was observed in **PA-BTD-Br** compared to that of **BP**. Unlike other compounds, the introduction of electron donating Si in **PA-BTD-TIPSA** produced a slightly increased E_{HOMO}, by 0.25 eV, compared to that of **PA-BTD-Br**, while still having a low E_{LUMO} of -3.87 eV.

Examination molecular orbitals allowed for a visualization of the π-extenders effects on E_{LUMO} and E_{HOMO}. In the case of the LUMO, the orbitals were localized on the more electron deficient portion of the molecule including the π-extenders. Conversely, the HOMO orbitals were found to localize on the more electron-rich portion of the molecule away from the π-extenders. Therefore, the electron-withdrawing ability of π-extenders reflected more on the E_{LUMO} than E_{HOMO}.

Additionally, nearly all compounds assembled into 1D fibrilar structures through either gelation or a PT assembly method despite their large π-cores. A partial crystal structure of **PA-BTD-TIPSA** showed an anti-parallel packing structure.

CHAPTER 2

COMPRESSION OF E_{gap} USING A DONOR-ACCEPTOR SYSTEM

2.1 Introduction

Low bandgap materials have been of particular interest on the development of intrinsically conductive materials[56] and most recently utility in organic solar cells.[3-5,57-59].

A low band gap was observed for polyisothianaphthene, which was 1 eV, was ascribed to the contribution of quinoidal structure in the ground state.[60,61,65] Many examples of this structure have been reported, and have shown impressively low E_{gap}. This method, however, does not provide independent control over both E_{HOMO} and E_{LUMO}.[65,67,68]

A more common approach to producing low band gap materials is the use of a donor-acceptor system which utilizes a structure containing an alternating electron-donor and electron-acceptor.[67] The motivation behind this method is the use of a structure containing units having a low-ionization potential (increased E_{HOMO}) and units having a large electron affinity (decreased E_{LUMO}). Hybridization of E_{HOMO} and E_{LUMO} of each the donor, and the acceptor units lead to an overall compression of E_{gap}. Theoretical studies on donor-acceptor systems have revealed that LUMO orbitals primarily lie on the acceptor portion of the molecule, and HOMO orbitals are delocalized throughout the entire molecule.[68] Such delocalization of HOMO orbitals has been found to be significantly affected by the torsional (dihedral) angle between the donor and acceptor units.[68-73]

Due to the large variety of donor and acceptor units available, multiple examples of donor-acceptor polymers have been reported.[3-5,68-75] Use of electron-rich thiophene as

the donor unit is very common.[70,75,78-82] Although formation of a thin film may be more challenging, small molecule donor-acceptor systems have recently emerged as attractive materials.[57,76-77] Benefits such as synthetic reproducibility and the ability to self-assemble into ordered structures have encouraged more studies on small-molecule systems.

For system II, a series of donor-acceptor small-molecules have been designed based on pyrazine-acene (**PA**) as the acceptor, and thiophene (**TH**) as the donor. (Figure 2.1) A comparison between two base **PA** π-cores, phenazine and bisphenazine will be described. As observed in system I (Chapter 1), extension of the π-core with an electron-deficient thiadiazole (**TD**) unit dramatically lowered E_{LUMO} of a bisphenazine based core. Using this knowledge, we also synthesized phenazine and bisphenazine π-cores that have been extended with a **TD** unit to further enhance the electron-deficiency of the acceptor unit.

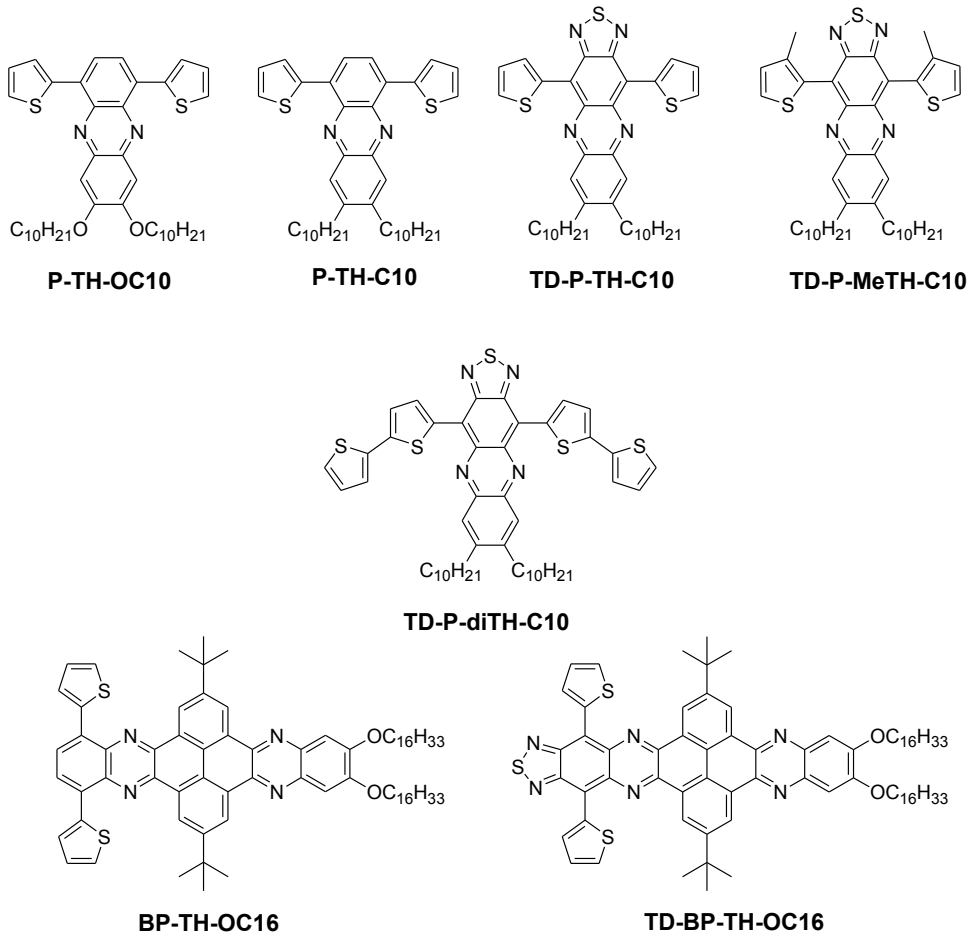

Figure 2.1. Low E_{gap} compounds based on a thiophene donor and pyrazine-acene (**PA**) acceptor (system II).

To better understand the role of the dihedral angle in E_{HOMO} control, a compound containing a methylated thiophene is also presented. The presence of the bulky methyl group serves to disrupt the planarity of the molecule. A simplified system with truncated solubilizing groups was subjected to extensive theoretical evaluation to more thoroughly explain the role of the dihedral angle.

An additional thiophene has also been added to a **TD** extended phenazine to evaulate how the number of thiophene substituents affects the electronic properties.

Additionally, the type of solubilizing group (alkoxy vs. alkyl) is also evaluated for phenazine based compounds.

To test the ability to self-assemble into ordered structures, cast-films and phase transfer assembly were implemented for the small molecules presented.

2.2 Experiments

2.2.1 Instrumentation

Nuclear magnetic resonance (NMR) spectra were obtained with a Varian Gemini 400 MHz NMR spectrometer at room temperature. Deuterated chloroform ($CDCl_3$) containing tetramethylsilane (TMS) as an internal reference was used as the solvent for both ^1H NMR and ^{13}C NMR. Elemental Analysis was carried out by Atlantic Microlab, inc. Mass spectra were collected at the University of Illinois, Chicago. Optical properties of the molecules were obtained with Shimadzu UV-2600 UV-visible spectrophotometer and Horiba Fluorimeter using a xenon lamp excitation source for absorption and fluorescence emission, respectively. Electrochemistry measurements were performed with CV on a CH instrument 660D with a three electrode configuration, with a cell equipped with a platinum plate as the counter electrode, a platinum disc as the working electrode (2 mm diameter), and a non aqueous Ag/Ag^+electrode (Ag in 10 mM $AgNO_3$ solution in anhydrous acetonitrile) as the reference electrode. CV measurements for all compounds were recorded in a methylene chloride solution containing 0.1 M tetrabutylammonium hexafluorophosphate ($TBAPF_6$) as the supporting electrolyte. All solutions were purged with Ar for 20-30 min before each experiment, and a positive pressure of Ar was maintained over the sample solution during the experiments. The scan rate was ν = 100 mV/s for all experiments. All potentials are reported versus the

ferrocene/ferrocenium (Fc/Fc^+) redox couple which was used as an internal standard 6-10 drops of an 8 mM solution in methylene chloride). TEM experiments were performed using a Tecnai G2 F30 S-Twin TEM with a 300 KeV Schottky field emission gun. Samples were prepared as described in Figure 2.10, and gently dropped onto a Lacey Formvar/Carbon, 200 mesh copper grid using a pipette and allowed to air dry while kept covered in a glass petri dish.

2.2.2 Synthetic Procedures

All chemicals were purchased from commericial sources and used as received without further purification. The diketophenazine intermediate[45], 5,6-diamino-4,7-dithien-2-yl-2,1,3-benzothiadiazole[82], 3,6-di-thiophen-2-yl-benzene-1,2-diamine[69], 3-methyl-2-tributylstannylthiophene[83], 4,7-dibromo-5,6-dinitro-benzo[1,2,5]thiadiazole[3], 4,5-Bis-decyl-benzene-1,2-diol[84], and 5-(tributylstannyl)-2,2-bithiophene[85] were prepared according to previously published procedures.

P-TH-OC10 0.461 mmol dibromo-phenazine[86] was added to a round bottom flask containing 1 mol% $PdCl_2(PPh_3)_2$. 15 mL of THF degassed with nitrogen was added to the reaction flask followed by 1.01 mmol 2-(tributylstannyl)thiophene. Reflux under nitrogen, overnight. An additional 4 mol % of Pd catalyst was added to the reaction mixture which was then allowed to stir, refluxing overnight. The resulting solution was evaporated onto silica gel allowing the pure product to be obtained by silica gel chromatography (20 % CH_2Cl_2 in hexane) providing 66 % yield. ^1H NMR (400 MHz, $CDCl_3$, ppm): δ 8.11 (2H, s), 7.96 (2H, dd, *J*=2.4 Hz), 7.54 (2H, dd, *J*=4.4 Hz), 7.43, (2H, s), 7.20 (2H, dd, *J*=3.6 Hz), 4.27 (4H, t, *J*=6.8 Hz), 1.89 (4H, m), 1.54-1.25 (28H, overlapping peaks), 0.89 (6H, t, *J*=6.8 Hz) ^{13}C (100 MHz, $CDCl_3$, ppm) : 154.67,

140.65, 139.47, 138.51, 131.18, 128.12, 126.71, 126.58, 125.99, 105.66, 69.33, 31.94, 29.65, 29.59, 29.40, 29.38, 28.86, 26.07, 22.71, 14.13. $[M+H]^+$: Calcd: 656.4 Found: 657.4

4,5-bis-decyl-[1,2]benzoquinone 0.998 mmol 4,5-Bis-decyl-benzene-1,2-diol was placed in a 20 mL vial containing 5.99 mmol of sodium sulfate. 15 mL of $CHCl_3$ was added to the vial followed by 2.99 mmol of Silver oxide. The reaction vial was quickly covered to exclude light, and stirred for 1 hour, under nitrogen. The resulting solution was passed through a 0.2 μm PTFE filter directly into the reaction flask for the subsequent cyclization reaction without further characterization or purification.

P-TH-C10 6 mL of acetic acid was put into a round bottom flask containing 0.499 mmol of 3,6-di-thiophen-2-yl-benzene-1,2-diamine. 0.499 mmol of 4,5-bis-decyl-[1,2]benzoquinone in 8 mL $CHCl_3$ was added into the reaction flask. An additional 11 mL of $CHCl_3$ was added. The reaction mixture was refluxed under nitrogen for 1 hour. The resulting solution was extracted into chloroform and washed with 5% NaOH, then water and dried over sodium sulfate. Column chromatography (10 % CH_2Cl_2 in hexane) provided the pure compound in 36% yield. ^{1}H NMR (400 MHz, $CDCl_3$, ppm): δ 8.16 (2H, s), 8.10 (2H, s), 7.99 (2H, dd, *J*=1.2 Hz), 7.55 (2H, dd, *J*=1.2 Hz), 7.23, (2H, dd, *J*= 3.6 Hz), 2.90 (4H, t, *J*=8.0 Hz), 1.80 (4H, m), 1.54-1.25 (28H, overlapping peaks), 0.88 (6H, t, *J*=7.0 Hz) ^{13}C (100 MHz, $CDCl_3$, ppm): 146.26, 141.41, 139.85, 139.20, 131.68, 128.45, 127.42, 126.73, 126.68, 33.18, 31.91 30.53, 29.81, 29.64, 29.62, 29.56, 29.35, 22.69, 14.11 (1 aromatic peak not seen due to overlapping signals). $[M+H]^+$: Calcd: 624.4 Found:625.4

BP-TH-OC16 4 mL of acetic acid was put into a round bottom flask containing 0.330 mmol of 3,6-di-thiophen-2-yl-benzene-1,2-diamine, and 0.275 mmol of diketophenazine in 12 mL $CHCl_3$ was added into the reaction flask. The reaction mixture was refluxed under nitrogen for 1 hour. The resulting precipitate was filtered and washed with water and methanol. Column chromatography ($CHCl_3$) provided the pure compound in 64% yield. ^{1}H NMR (400 MHz, $CDCl_3$, ppm) δ 10.04 (2H, d, *J*=2.0 Hz), 9.77 (2H, d, *J*=2.4 Hz), 8.30 (2H, s), 8.00 (2H, dd, *J*=1.2 Hz), 7.69, (2H, dd, *J*=1.0 Hz), 7.63 (2H, s), 7.31 (2H, *J*=2.6 Hz), 4.33 (4H, t, *J*=6.6 Hz), 2.02 (4H, m), 1.79 (18H, s), 1.61 (4H, m), 1.49-1.26 (44H, overlapping peaks), 0.88 (6H, t, *J*=6.8 Hz) ^{13}C NMR was unable to be performed due to poor solubility at concentrations required for ^{13}C NMR measurements. Elemental Analysis: Calculated: C, 78.44; H, 8.49; N, 4.81; S, 5.51 Found: C, 78.49; H, 8.59; N, 4.75; S, 5.37.

TD-P-TH-C10 5 mL of acetic acid was put into a round bottom flask containing 0.385 mmol of 5,6-diamino-4,7-dithien-2-yl-2,1,3-benzothiadiazole. 0.385 mmol of 4,5-bis-decyl-[1,2]benzoquinone in 5 mL $CHCl_3$ was added into the reaction flask. An additional 10 mL of $CHCl_3$ was added. The reaction mixture was refluxed under nitrogen for 1 hour. The resulting solution was extracted into $CHCl_3$, and washed with $NaHCO_3$, then water and dried over sodium sulfate. Column chromatography (CH_2Cl_2) followed by precipitation from CH_2Cl_2 into methanol provided the pure compound in 58% yield. ^{1}H NMR (400 MHz, $CDCl_3$, ppm) δ 9.12 (2H, d, *J*=3.6 Hz), 7.97 (2H, s), 7.73 (2H, d, *J*=5.2 Hz), 7.36 (2H, t, *J*=4.4 Hz), 2.87 (4H, t, *J*=7.6 Hz), 1.81 (4H, m), 1.54-1.25 (28H, overlapping peaks), 0.89 (6H, t, *J*=6.6 Hz) ^{13}C (100 MHz, $CDCl_3$, ppm) 151.06, 148.13, 143.17, 136.94, 136.90, 133.33, 131.64, 126.92, 120.91, 105.02, 33.31, 31.93, 30.30,

29.82, 29.66, 29.65, 29.58, 29.36, 22.70, 14.31. Elemental Analysis: Calculated: C, 70.34; H, 7.38; N, 8.20; S, 14.08 Found: C, 69.86; H, 7.27; N, 8.05; S, 13.75.

TD-BP-TH-OC16 To a round bottom flask containing 0.303 mmol of diketophenazine, $CHCl_3$ (12 mL) and acetic acid (4 mL) were added. 0.363 mmol of 5,6-diamino-4,7-dithien-2-yl-2,1,3-benzothiadiazole was added to the flask lastly. The resulting solution was stirred, under a nitrogen atmosphere, at 90°C for 18 hours. Precipitates obtained after cooling the reaction solution were filtered and rinsed with $NaHCO_3$, H_2O and methanol. The crude product was attached to neutral alumina, and washed with CH_2Cl_2 through a column and then recovered by filtering the attached alumina with hot chloroform to provide a yield of 92% ^{1}H NMR (400 MHz, $CDCl_3$, ppm) δ 9.98 (2H,s), 9.74 (2H, s), 9.10 (2H, d, *J*=3.6 Hz), 7.81 (2H, d, *J*=5.2 Hz), 7.61 (2H, s), 7.43 (2H, t, *J*=4.2 Hz), 4.33 (4H, t, *J*=6.4 Hz), 2.02 (4H, m), 1.79 (18H, s), 1.61 (4H, m), 1.49-1.26 (44H, overlapping peaks), 0.88 (6H, t, *J*=6.6 Hz) ^{13}C NMR was unable to be performed due to poor solubility at concentrations required for ^{13}C NMR measurements. Elemental Analysis: Calculated: C, 74.71; H, 7.92; N, 6.88; S, 7.87 Found: C, 74.71; H, 7.75; N, 6.85; S, 7.81.

4,7-bis-(3-methyl-thiophen-2-yl)-5,6-dinitro-benzo[1,2,5]thiadiazole To a round bottom flask containing 5.70 mmol of 3-methyl-2-tributylstannylthiophene, 1.90 mmol of 4,7-dibromo-5,6-dinitro-benzo[1,2,5]thiadiazole was added. 10 mL of degassed THF was added, followed by 3 mol% $PdCl_2(PPh_3)_2$. The solution was refluxed under nitrogen for 24 hours. Column chromatography (30% CH_2Cl_2 in hexane) gave the desired product in 55% yield. ^{1}H NMR (400 MHz, $CDCl_3$, ppm) δ 7.57 (2H, d, *J*=5.2 Hz), 7.07 (2H, d, *J*=5.2 Hz), 2.18 (6H, s).

4,7-bis-(3-methyl-thiophen-2-yl)-5,6-diamino-benzo[1,2,5]thiadiazole 12.6 mmol of iron powder was put in a round bottom flask containing 1.05 mmol 4,7-bis-(3-methyl-thiophen-2-yl)-5,6-dinitro-benzo[1,2,5]thiadiazole in 20 mL acetic acid. The solution was stirred, under nitrogen at 90°C for 5 hours. The mixture was poured into water, and the product was extracted into ether, washed with $NaHCO_3$, and dried over $MgSO_4$. After drying, a gold solid was obtained and used without further purification. ^1H NMR (400b MHz, $CDCl_3$, ppm) δ 7.48 (2H, d, *J*=5.2 Hz), 7.10 (2H, d, *J*=5.2 Hz), 4.13 (4H, s), 2.14 (6H, s)

TD-P-MeTH-C10 13 mL of acetic acid was put into a round bottom flask containing 1.05 mmol of 4,7-bis-(3-methyl-thiophen-2-yl)-5,6-diamino-benzo[1,2,5]thiadiazole. 1.05 mmol of 4,5-bis-decyl-[1,2]benzoquinone in 16 mL $CHCl_3$ was added into the reaction flask. An additional 20 mL of $CHCl_3$ was added. The reaction mixture was refluxed under nitrogen for 1 hour. The resulting solution was extracted into $CHCl_3$, and washed with $NaHCO_3$, then water and dried over sodium sulfate. Column chromatography (40% methylene chloride in hexane) provided the pure compound in 65% yield. ^1H NMR (400 MHz, $CDCl_3$, ppm) δ 7.82 (2H, s), 7.67 (2H, d, *J*=4.8 Hz), 7.22 (2H, d. *J*=5.2 Hz), 2.80 (4H, t, *J*=7.8 Hz), 2.19 (6H, s), 1.75 (4H, M), 1.45-1.28 (28H, overlapping peaks), 0.88 (6H, t, *J*=6.6 Hz) ^{13}C (100 MHz, $CDCl_3$, ppm) δ 152.58, 148.03, 144.66, 139.50, 139.17, 130.52, 130.35, 127.58, 127.49, 123.99, 33.17,31.92, 30.06, 29.77, 29.63, 29.59, 29.54, 29.35, 22.70, 16.35, 14.12. $[M+H]^+$: Calcd: 710.35 Found: 711.5

4,7-Bis-[2,2']bithiophenyl-5-yl-5,6-dinitro-benzo[1,2,5]thiadiazole 0.781 mmol 4,7-dibromo-5,6-dinitro-2,1,3-benzothiadiazole was added to a round bottom flask

followed by 1 mol% $PdCl_2(PPh_3)_2$. 1.64 mmol of 5-(tributylstannyl)-2,2-bithiophene was diluted in 6 mL degassed THF and added to the reaction flask via syringe. This reaction mixture was refluxed for 24 hours. The resulting solution was evaporated and the solid was washed with methanol and hexane. Column chromatography (methylene chloride) provided the product in 72% yield. ^{1}H NMR (400 MHz, $CDCl_3$, ppm) δ 7.46 (2H, d, *J*= 3.6 Hz), 7.34 (4H, d, *J*=4.4 Hz), 7.28 (2H, d, *J*=4.0 Hz), 7.08 (2H, m). ^{13}C NMR not performed due to limited solubility.

4,7-Bis-[2,2']bithiophenyl-5-yl-5,6-diamino-benzo[1,2,5]thiadiazole 2.17 mmol of iron powder was put in a round bottom flask containing 0.180 mmol 4,7-Bis-[2,2']bithiophenyl-5-yl-5,6-dinitro-benzo[1,2,5]thiadiazole in 10 mL acetic acid. The solution was stirred, under nitrogen at 90°C for 5 hours. The mixture was poured into water, and the product was extracted into ether, washed with $NaHCO_3$, and dried over $MgSO_4$. After drying, a gold solid was obtained and used without further purification or characterization.

TD-P-diTH-C10 2 mL Acetic acid was added to a round bottom flask containing 0.180 mmol 4,7-Bis-[2,2']bithiophenyl-5-yl-5,6-diamino-benzo[1,2,5]thiadiazole. 0.180 mmol of 4,5-bis-decyl-[1,2]benzoquinone in 8 mL $CHCl_3$ was added into the reaction flask. The solution was refluxed under nitrogen overnight. The resulting precipitates were filtered and washed with methanol, ethyl acetate, and hexane. Column chromatography provided the pure compound in 30% yield. ^{1}H NMR (400 MHz, $CDCl_3$, ppm) δ 9.08 (2H, d, *J*=4.4 Hz), 7.89 (2H, s), 7.45 (2H, d, *J*=3.6 Hz), 7.36 (2H, d, *J*=4.0 Hz), 7.33 (2H, d, *J*=5.2 Hz), 7.14 (2H, m), 2.84 (4H, t, *J*=7.8 Hz), 1.82 (4H, m), 1.56-1.29 (28H, overlapping peaks), 0.89 (6H, t, *J*=6.8 Hz). ^{13}C NMR was not

performed due to limited solubility. Elemental Analysis: Calculated: C, 68.04; H, 6.42; N, 6.61; S, 18.92 Found: C, 67.90; H, 6.31; N, 6.62; S, 18.92.

2.2.3 Cast film preparation

A diluted solution of each compound was used to produce cast films. The solution was drop cast onto a clean glass slide for POM studies and allowed to slowly dry while undisturbed.

2.2.4 Precipitation

A concentrated solution compound $CHCl_3$ is heated until homogeneous. While cooling to room temperature, solids come out of solution. In comparison to recrystallization, this should be a relatively fast process.

2.2.5 Phase Transfer Assembly

A binary solvent system with methylene chloride and methanol was used for PT assembly of **TD-BP-TH-OC16**. All solvents were filtered through a 0.2 µm PTFE filter before each experiment. Each compound was dissolved in methylene chloride and filtered into a clean 20 mL screw cap vial. Filtered methanol was slowly added so that two phases could be maintained. The mixture was left undisturbed overnight to promote 1D assembly. A variety of concentrations were tested as well as various volume ratios of methylene chloride/methanol.

2.3 Results and Discussion

2.3.1 Synthesis

The synthetic routes to the target molecules are summarized in Scheme 2.1. In general, the thiophene-pyrazine-acenes were prepared via two approaches: (1) a

condensation reaction between a thiophene containing diamine with a diketo compound or (2) Stille coupling between a dibromopyrazine-acene and a stannylated thiophene.

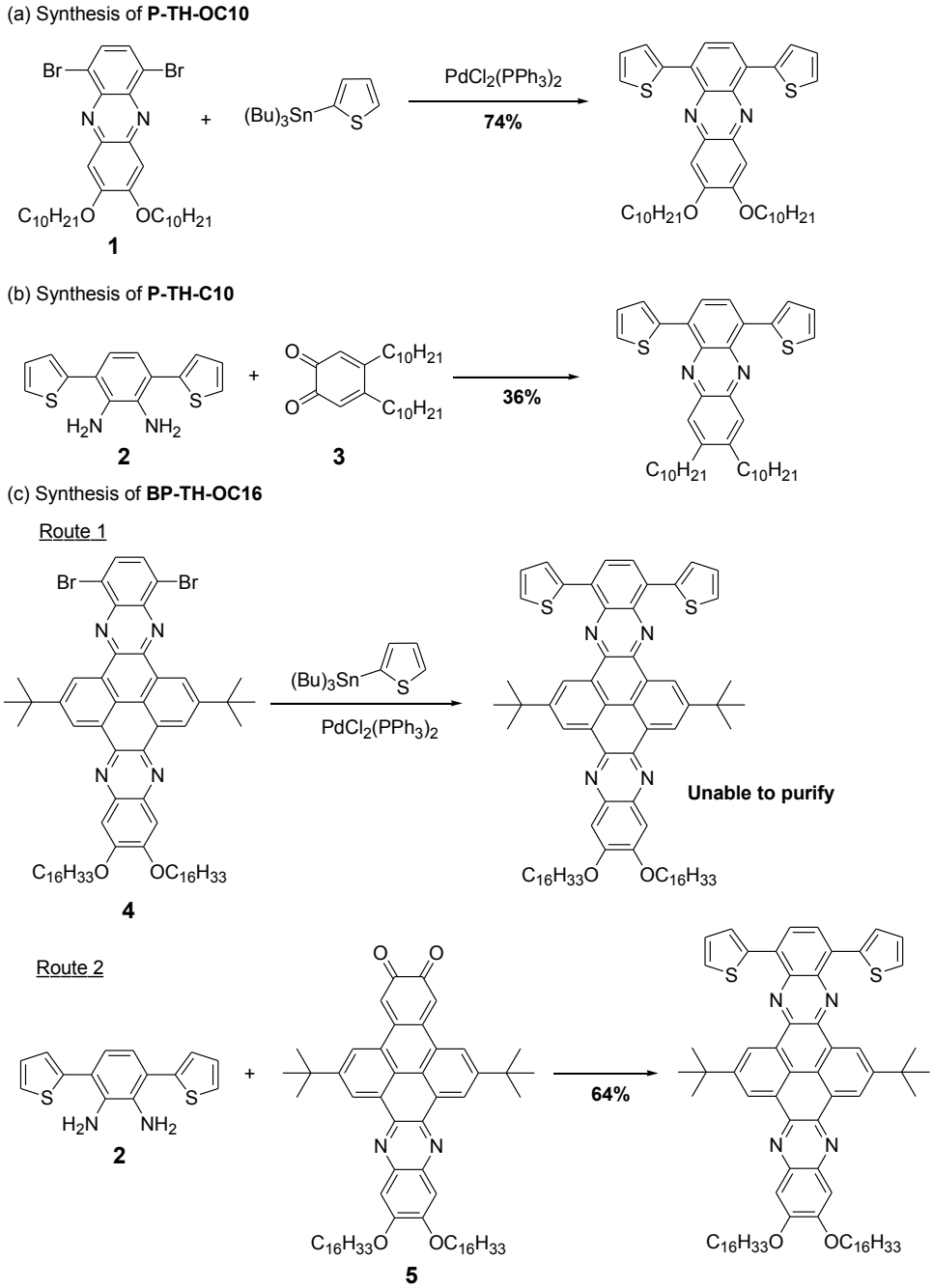

Scheme 2.1(a). Synthetic routes to the target **PA-TH** molecules.

(d) Synthesis of **TD-P-TH-OC10**

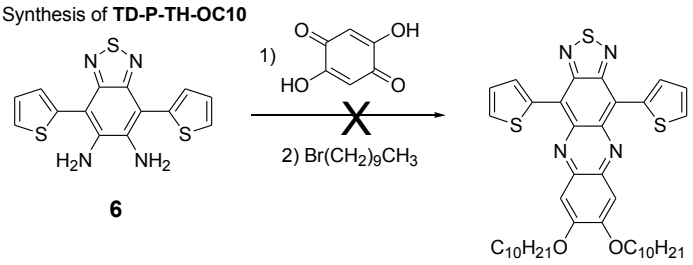

(e) Synthesis of **TD-P-TH-C10**

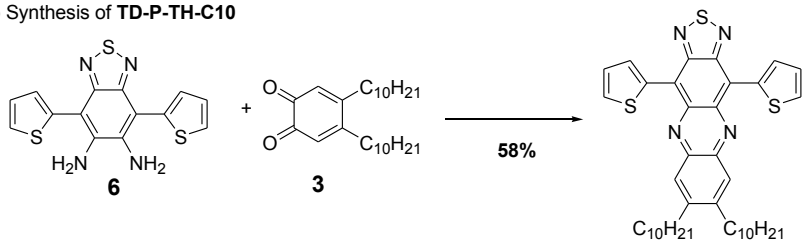

(f) Synthesis of **TD-P-MeTH-C10**

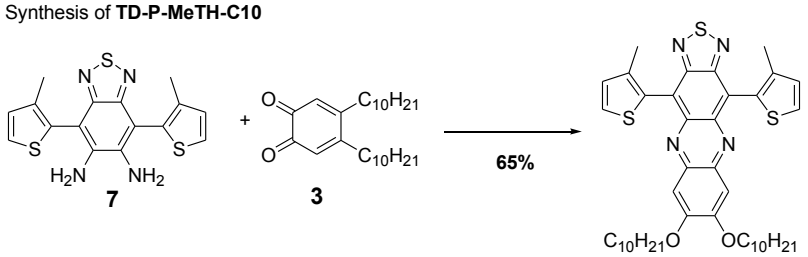

(g) Synthesis of **TD-BP-TH-OC16**

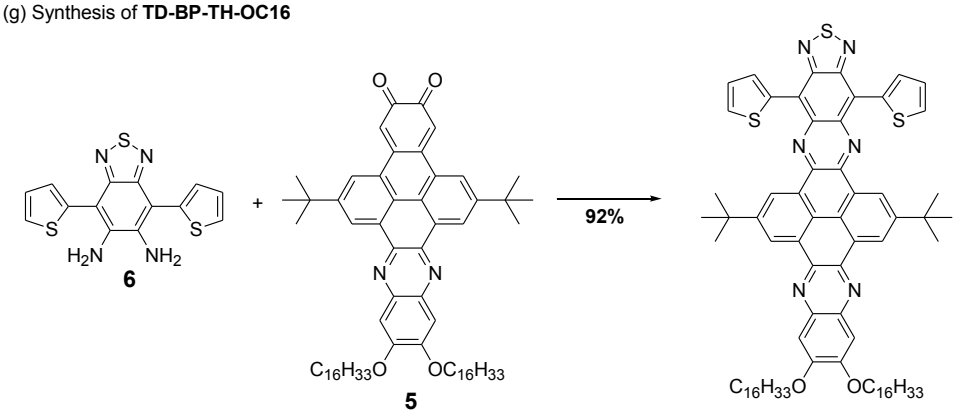

Scheme 2.1(b). Synthetic routes to the target **PA-TH** molecules.

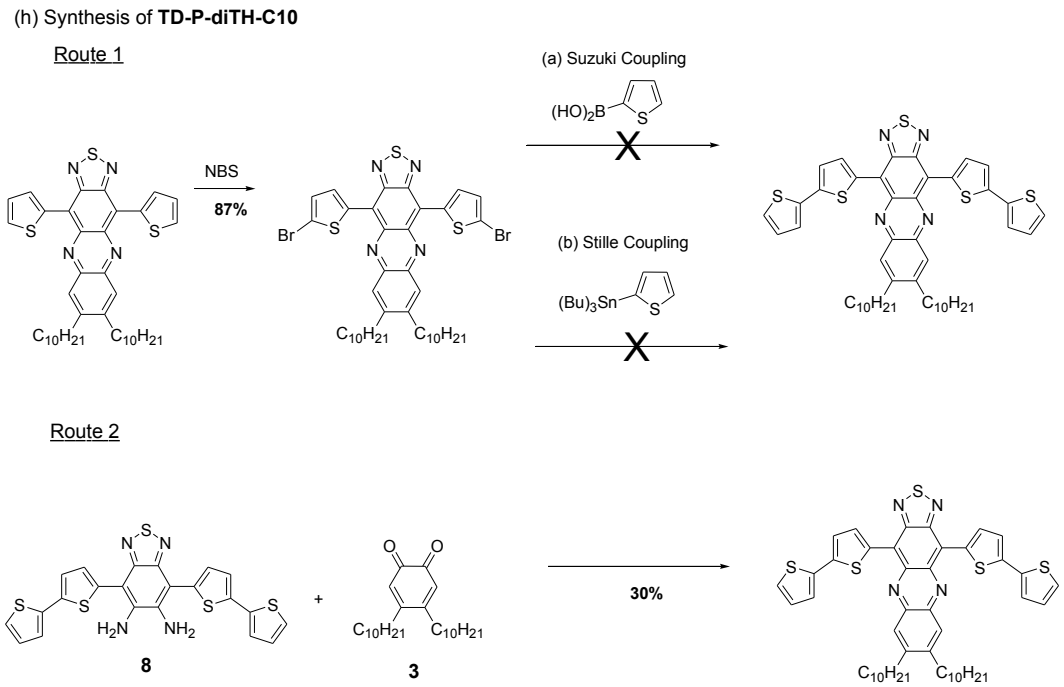

Scheme 2.1(c). Synthetic routes to the target **PA-TH** molecules.

Stille coupling between 1,4-dibromo-7,8-bis(decyloxy)phenazine (**1**) and 2-(tributylstannyl)thiophene with a catalytic amount of $PdCl_2(PPh_3)_2$ afforded **P-TH-OC10** with a yield of 74%. Meanwhile, **P-TH-C10** was prepared by a condensation reaction between 1,2-diamino-3,6-dithien-2-ylbenzene (**2**) and highly reactive 4,5-bis-decyl-[1,2]benzoquinone (**3**). A Stille coupling between the dibromobisphenazine **4** and 2-(tributylstannyl)thiophene to prepare **BP-TH-OC16** was unsuccessful due to the presence of inseparable impurities. Alternatively, a condensation reaction between the diamine **2** and diketophenazine **5** was successful to afford 64% yield.

To prepare **TD-P-TH-OC10**, two approaches were tested: (i) a reaction between 5,6-diamino-4,7-dithien-2-yl-2,1,3-benzothiadiazole (**6**) and 2,5-dihydroxy-1,4-benzoquinone followed by a Williamson ether synthesis with bromodecance and (ii) a cyclization between 5,6-diamino-4,7-dibromo-2,1,3-benzothiadiazole and 2,5-dihydroxy-1,4-benzoquinone, followed by a Williamson ether synthesis with bromodecane, a then a

Stille coupling with 2-(tributylstannyl)thiophene. However, both approaches were unsuccessful and therefore, we were unable to synthesize **TD-P-TH-OC10**. Alternatively, when diamine **6** was reacted with diketone **3**, **TD-P-TH-C10** (with decyl rather than decyloxy substituents) was successfully prepared with a yield of 58%.

To synthesize **TD-P-MeTH-C10**, 3-methyl-2-tributylstannylthiophene was reacted with 4,7-dibromo-5,6-dinitro-2,1,3-benzothiadiazole under a Stille coupling condition with $PdCl_2(PPh_3)_2$ and then the resulting dinitro product was reduced to over Fe to afford diamine **7**. A condensation of diamine **7** and diketone **3** produced **TD-P-MeTH-C10** in 65% yield as a viscous green liquid. Finally, **TD-BP-TH-OC16** was obtained from a condensation of diamine **6** with diketophenazine **5**.

Bromination of **TD-P-TH-C10** with NBS was successful in giving **TD-P-THBr-C10**, however, subsequent coupling reactions failed. Suzuki coupling was attempted using 2-thienylboronic acid without giving the desired product. Similarly, Stille coupling with 2-(tributylstannyl)thiophene failed to provide **TD-P-diTH-C10**. As shown in route 2, Stille coupling between 4,7-dibromo-5,6-dinitro-2,1,3-benzothiadiazole and 5-(tributylstannyl)-2,2-bithiophene was attempted, and successfully gave the desired dinitro intermediate, which was reduced to give diamine **8.** Cyclization of this diamine with diketone **3** gave **TD-P-diTH-C10** in 30% yield.

2.3.2 Physical Properties

2.3.2.1 Optical Properties

The $CHCl_3$ solutions of the **PA-TH** molecules exhibited a wide range of color from yellowish orange to green. An early interesting comparison can be made from this color pattern between the smaller and larger π-cores (**P-TH-OC10** / **P-TH-C10** versus

BP-TH-OC16 and **TD-P-TH-C10** / **TD-P-MeTH-C10** versus **TD-BP-TH-OC16**). Interestingly and unexpectedly, thiophene-pyrazine-acenes with smaller π-cores showed longer wavelength absorbing colors than their larger versions.

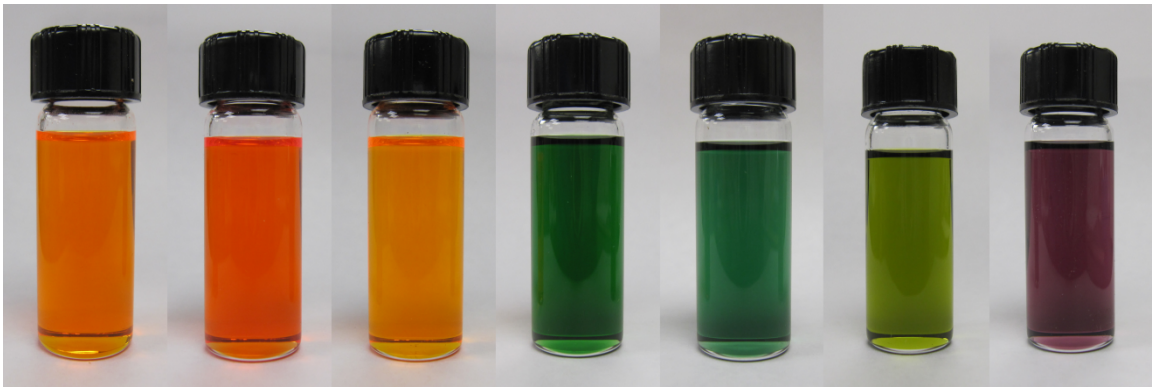

Figure 2.2. Chloroform solutions (from left to right) of **P-TH-OC10**, **P-TH-C10**, **BP-TH-OC16**, **TD-P-TH-C10**, **TD-P-CH$_3$TH-C10**, **TD-P-diTH-C10** and **TD-BP-TH-OC16.**

The UV-Vis spectra of system II **PA-TH**s showed absorptions characteristic to the **PA** π-cores (ca. 400 – 420 nm) and additional peaks at longer wavelengths which are presumed to be due to the extension of π-conjugation by addition of thiophene substituents. **P-TH-OC10** showed two major absorptions at 405 nm and 465 nm. When the decyloxy side groups were replace by decyl side groups (**P-TH-C10**), the peak at 405 nm was blue-shifted to 385 nm, while the peak at 465 nm was red-shifted to 485 nm. This is a notable change considering the minimal structural change in these two compounds. Despite having a larger **PA** core, **BP-TH-OC16** did not show a discernible second absorption. **TD-P-TH-C10** showed quite an interesting absorption behavior. The absorption from the π-core at 405 nm did not change when compared to **P-TH-OC10**, the

second absorption was shifted to 745 nm. When the thiophene was substituted with methyl group (**TD-P-MeTH-C10**), the second absorption was blue-shifted to 625 nm. This is hypothesized to be due to the steric hindrance caused by the methyl substituents which may force the thiophene out-of-plane with respect to the **P** core. When an additional thiophene unit is added to the **TD-P-TH-C10** based core, **TD-P-diTH-C10**, a dramatic shift (from 745 nm to 880 nm) in the second absorption maximum was observed. The compound with the largest π-core (**TD-BP-TH-C16**) exhibited λ_{max} at 678 nm which is still shorter than that of **TD-P-TH-C10** which has a smaller π-core.

From the tangent of the absorption edge of the UV Vis spectrum, E_{gap} can be calculated. These values are summarized in Table 2.2. With the substitution of alkoxy (**P-TH-OC10**) side groups to alkyl (**P-TH-C10**) side groups a difference in E_{gap} of 0.09 eV was observed. Interestingly, the E_{gap} of **BP-TH-OC16** was nearly identical to that of **P-TH-OC10** (2.27 eV and 2.28 eV, respectively). Significant compression was observed when the **PA** core was extended with by the **TD** moiety. In the case of **TD-BP-TH-OC16**, an E_{gap} of 1.55 eV was calculated. This is significantly decreased compared to the E_{gap} of **BP-TH-OC16** with a difference of 0.72 eV. Furthermore, the smaller **P** systems containing a **TD** unit showed even more significant compression of E_{gap}. **TD-P-TH-C10**'s E_{gap} was calculated to be 1.43 eV, however, with the introduction of the bulky methyl substituent (**TD-P-MeTH-C10**) an increase in E_{gap} of 0.27 eV was observed. A more thorough evaluation of this observation is discussed in section 2.3.3. The most significant compression of E_{gap} to 1.21 eV was obtained when an additional thiophene was added to the compound, **TP-P-diTH-C10**.

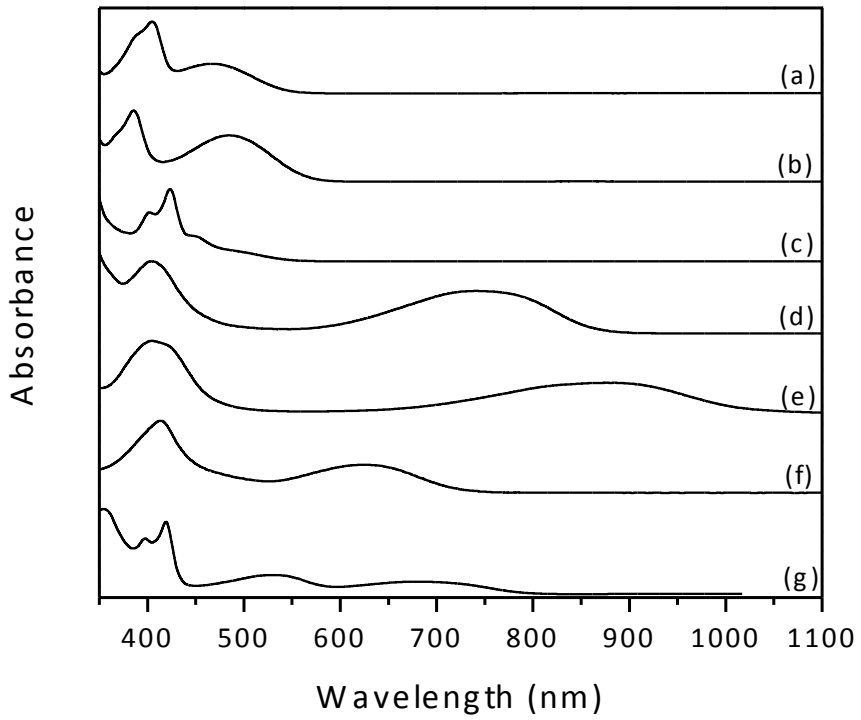

Figure 2.3. UV-Vis spectra of the system II molecules: (a) **P-TH-OC10**, (b) **P-TH-C10**, (c) **BP-TH-OC16**, (d) **TD-P-TH-C10**, (e) **TD-P-diTH-C10**, (f) **TD-P-MeTH-C10**, and (g) **TD-BP-TH-OC16** in $CHCl_3$.

The fluorescence of **PA**s without a **TD** moiety was significant giving quantum yields ranging from 0.17 to 0.29 using diphenylanthracene as the standard. However, **TD-PA**s did not show noticeable fluorescence. The molar absorptivity and fluorescence quantum efficiency for the **PA-TH**s are summarized in Table 2.1.

Table 2.1. Molar absorbtivity and Fluorescence quantum efficiency of system II.

	ε (at λ_{max}, $M^{-1}cm^{-1}$)	**Φ_F[a]**
P-TH-OC10	2.7×10^4 (405 nm)	0.29
BP-TH-OC16	6.1×10^4 (423 nm)	0.22
P-TH-C10	2.1×10^4 (385 nm)	0.17
TD-P-TH-C10	2.1×10^4 (405 nm)	NA[b]
TD-BP-TH-OC16	8.7×10^4 (419 nm)	NA[b]
TD-P-MeTH-C10	1.7×10^4 (413 nm)	NA[b]
TD-P-diTH-C10	5.7×10^4 (407 nm)	NA[c]

[a] Measured with diphenyl anthracene as a standard (Φ_F=0.90), excitation at 360 nm.
[b] Unable to determine accurate efficiency ($\Phi_F < 0.05$) [c] Not measured.

2.3.2.2 Electrochemical Properties

The electronic properties of the **PA-TH**s are summarized in Table 2.2. The experimental E_{HOMO} (E_{HOMO}^{EXP}) was obtained by subtracting E_{gap} (from the absorption edge) from E_{LUMO} (from CV) due to difficulty in direct characterization using CV.

When alkyl side chains were used rather than alkoxy side chains, a difference of 0.15 eV was observed, with **P-TH-C10** having a lower E_{LUMO} value. This can be attributed to the stronger electron donating effect from oxygen containing alkoxy groups in **P-TH-OC10**, which would lessen the electron deficiency of the acceptor unit.

It was found that significant decrease in E_{LUMO} was observed from **TD-TH-PA**s when compared to non-**TD-TH-PA**s. Both **P** and **BP** based compounds showed a reduction in E_{LUMO} of ca. 0.50 eV with extension of the π-core with **TD**. An interesting finding that deserves a special note is that the lowest E_{LUMO} was from **TD-P-diTH-C10** (-3.94 eV) rather than **TD-BP-TH-OC16** (-3.84 eV) which contains the highest number of electron-deficient imine nitrogens.

For the more electron deficient **TD-PA**s, an opposite effect, compared to **PA**s not extended with **TD**, on E_{LUMO} is observed when **P** is used as the π-core rather than **BP**.

The phenazine based compound, **TD-P-TH-C10**, decreased E_{LUMO} only slightly (0.06 eV) than the **BP** based counterpart. For **P-TH-OC10** and **BP-TH-OC16**, the **BP** had E_{LUMO} lowered by 0.13 eV.

The effect on E_{LUMO} when an additional thiophene unit is added (**TD-P-diTH-C10**) was almost negligible when compared to **TD-P-TH-C10**, with a difference in E_{LUMO} of only 0.04 eV. In this case, it was E_{HOMO} that was more affected by the addition of another thiophene. As seen in Table 2.2, E_{HOMO} was increased by 0.18 eV with this addition.

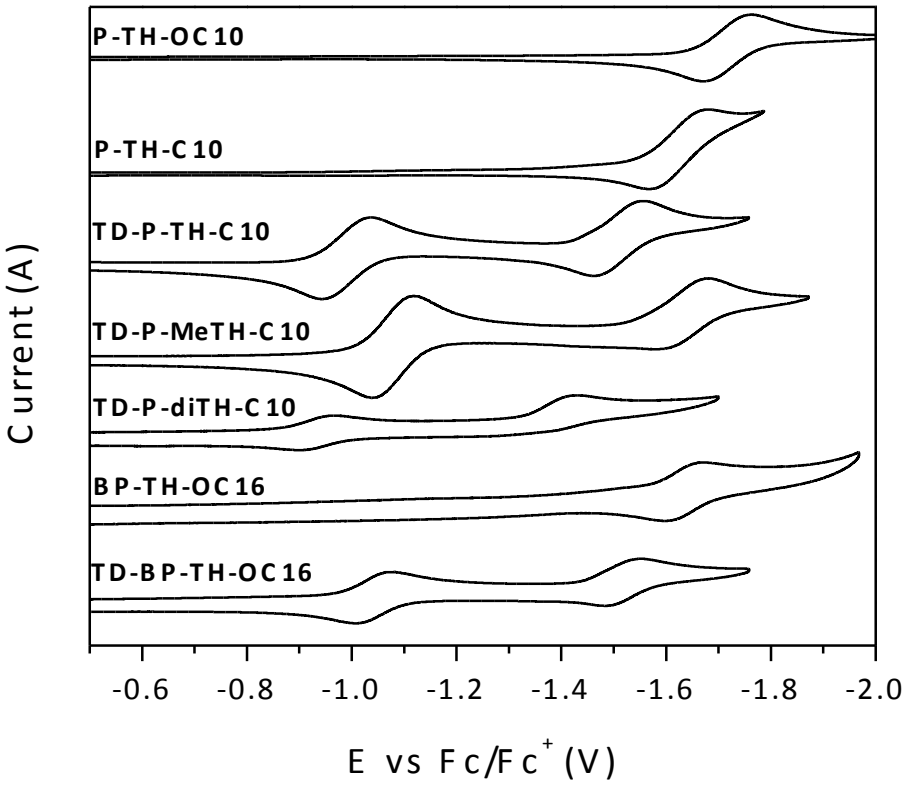

Figure 2.4. Cyclic voltammograms of the **PA-TH**s.

Table 2.2. Experimental and theoretical[a] electronic properties of the **PA-TH**s.

	E_{LUMO}^{EXP} [b]	E_{HOMO}^{EXP} [c]	E_{gap}^{EXP} [d]	E_{LUMO}^{THEO} [e]	E_{HOMO}^{THEO} [e]	$S_1^{Vertical}$[f]
P-TH-OC10	-3.17 eV	-5.45 eV	2.28 eV	-2.64 eV	-5.27 eV	2.29 eV
P-TH-C10	-3.32 eV	-5.51 eV	2.19 eV	-2.80 eV	-5.33 eV	2.17 eV
BP-TH-OC16	-3.30 eV	-5.57 eV	2.27 eV	-2.63 eV	-5.48 eV	2.48 eV
TD-P-TH-OC10	NA	NA	NA	-3.46 eV	-5.07 eV	1.41 eV
TD-P-TH-C10	-3.90 eV	-5.33 eV	1.43 eV	-3.62 eV	-5.13 eV	1.31 eV
TD-P-diTH-C10	-3.94 eV	-5.15 eV	1.21 eV	NA	NA	NA
TD-P-MeTH-C10	-3.80 eV	-5.50 eV	1.70 eV	-3.50 eV	-5.38 eV	1.60 eV
TD-BP-TH-OC16	-3.84 eV	-5.39 eV	1.55 eV	-3.43 eV	-5.24 eV	1.57 eV

[a]For theoretical evaluation, side groups were reduced to methoxy for decyloxy / hexadecyloxy and methyl for decyl, [b]From CV, [c]E_{LUMO}^{EXP} - E_{gap}^{EXP}[d]from UV-Vis, [e]B3LYP/6-31G*//B3LYP/6-31+G*, [f]$S_0 \rightarrow S_1$ vertical transition. The transitions are all one electron with the highest HOMO-LUMO contribution, NA not available.

2.3.3 Theoretical Evaluation

A more thorough and systematic approach was taken for the theoretical evaluation of system II to fully understand the interesting electronic properties observed experimentally. First, the relationship between the dihedral angle and E_{HOMO} were evaluated. Four molecules (Figure 2.4) were evaluated for the initial theoretical evaluation in which alkyl side groups were shortened to methoxy (rather than decyloxy or hexadecyloxy), as the side groups were inert to the electronic properties.

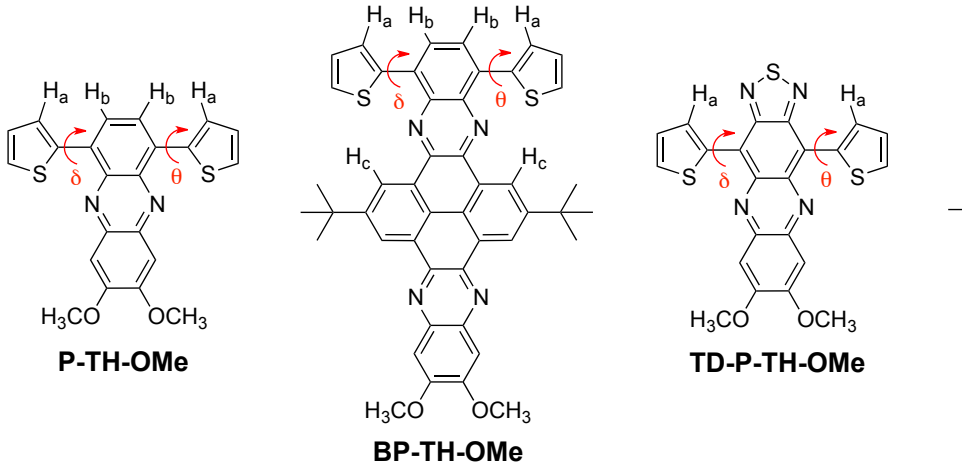

Figure 2.5. **PA-TH**s used in the theoretical study.

The highest calculated HOMO energies were observed for **TD-P-TH-OMe**. We note this system's optimized structure has a dihedral angle between thiophene and the π-core of 0°, thus producing the maximum π-orbital overlap between the substituents and the π-framework as summarized in Table 2.3. In this system, two attractive forces appear to contribute to a stable planar configuration: i) attraction between the thiophene-H (H_a) and thiadiazole-N and ii) thiophene-S and pyrazine-N. It should be noted that the nonbonding N···S interactions have been verified by previous crystallographic studies on TCNQ-TD[87] and TTF-oxazoline derivatives.[88] Theoretical investigations on 1,2,5-chalcogenadiazoles also supported such interactions.[89] In addition, a complete geometry and frequency analysis of **TD-P-TH-OMe** indicated a slight preference for the thiophene-S pointing toward pyrazine in the π-core. This was supported by the crystallographic data of a structurally analogous molecule.[69]

Table 2.3. Dihedral angles of thiophene-pyrazine-acenes with thiophene-S facing downward,interacting with pyrazine-N.

	P-TH-OMe	**BP-TH-OMe**	**TD-P-TH-OMe**	**TD-BP-TH-OMe**
Dihedral Angle	$\delta = 14.88^o$ $\theta = 14.88^o$	$\delta = 26.44^o$ $\theta = -26.64^o$	$\delta = 0.01^o$ $\theta = 0.01^o$	$\delta = 16.89^o$ $\theta = -16.89^o$

The lowest HOMO energy was found for **BP-TH-OMe**. Unlike the planar **TD-P-TH** system, this molecule's optimized geometry resulted in a dihedral angle between the thiophene and the π-core of ca. 26º ($\delta = 26.44^o$, $\theta = -26.64^o$). Two repulsions exist that we hypothesize are responsible for producing the largest dihedral angle of all systems studied: i) repulsion between H_a and H_b ii) repulsion between thiophene-S and H_c.

Interestingly, **P-TH-OMe** and **TD-BP-TH-OMe** have nearly the same dihedral angles ($\delta = 14.88^o$ vs $\delta = 16.89^o$, respectively), and nearly the same HOMO energies. The dihedral angles of these two molecules are in between our two extreme cases of planar and 27º, and as well, the HOMO energies of these two systems lie between the highest and lowest HOMO energy values. In each of these systems, we find one attractive force competing with a repulsive force. For **P-TH-OMe**, we hypothesize that the repulsion between H_a and H_b offsets the thiophene-S and pyrazine-N attractive force. In the case of **TD-BP-TH-OMe**, the repulsion between the thiophene-S and H_c appears to counterbalance the attractive forces existing in **TD-P-TH-OMe**. These competing attractive and repulsive interactions result in two molecules that lack planarity, and that have intermediate HOMO energies when compared to planar **TD-P-TH-OMe** and nonplanar **BP-TH-OMe**.

The impact of the dihedral angle on the HOMO and LUMO energies was investigated in greater detail by computationally determining the energy associated with a rotation of one of the thiophene substituents in **TD-P-TH-OMe**.

This analysis was carried out using the computationally expedient B3LYP/6-31G* level of theory with the focus on the relative energy difference rather than absolute values upon the rotation of the thiophene. We started with the optimized geometry for **TD-P-TH-OMe**, and commenced rotation of one thiophene, collecting single point energies at every 15° increment. As shown in Figure 2.6, the LUMO energy was unaffected by this rotation, while the HOMO energy decreased as the dihedral angle increased. The E_{gap} at 90° was 0.37 eV higher than that at 0°. The major contribution to this E_{gap} increase was E_{HOMO} decrease by 0.34 eV while E_{LUMO} was increased only by 0.03 eV. This computational result can be effectively illustrated by noting the specific localization of the HOMO and LUMO orbitals on **TD-P-TH-OMe**. Increased HOMO orbital coefficients are found on the more electron-rich thiophene-benzene-thiophene portion of the molecules, while the LUMO orbital coefficients are not significantly found on the thiophene. Note that the similar orbital localization has been observed in past computational studies.[68] The large HOMO orbital distribution on thiophene impacts the energy, which is significantly lowered upon out-of-plane thiophene rotation. In all of our systems, the HOMO orbital was found in this thiophene-benzene-thiophene region of the molecule.

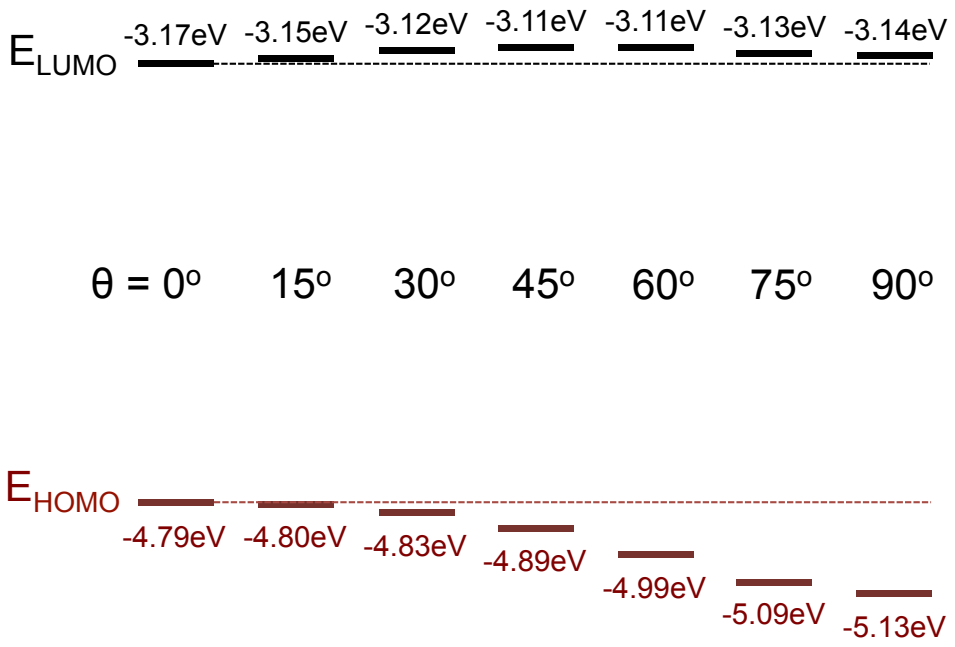

Figure 2.6. E_{HOMO} and E_{LUMO} as a function of dihedral angle between thiophene and **TD-P-TH-OMe** calculated by B3LYP/6-31G*.

Interestingly, E_{LUMO} for **P-TH-OMe** and **BP-TH-OMe** were nearly identical. The addition of **TD** on both systems (**TD-P-TH-OMe** and **TD-BP-TH-OMe**) significantly lowered E_{LUMO} by approximately 0.8 eV in both cases. An inspection of the LUMO orbital for **P-TH-OMe** and **BP-TH-OMe** showed localization on the same region of the molecule, i.e., **P** portion of both molecules (Figure 2.7). A similar orbital localization trend was found in **TD-P-TH-OMe** and **TD-BP-TH-OMe**, whereby LUMO coefficients also distributed on the **TD**, resulting in a lower energy when compared to the non-**TD** substituted version. This computational finding is consistent with the well-known, electron withdrawing nature of **TD**. We note that the previous discussion of planarity has no bearing on the LUMO energy of our systems, primarily because the thiophenes play an insignificant role in defining the LUMO orbital.

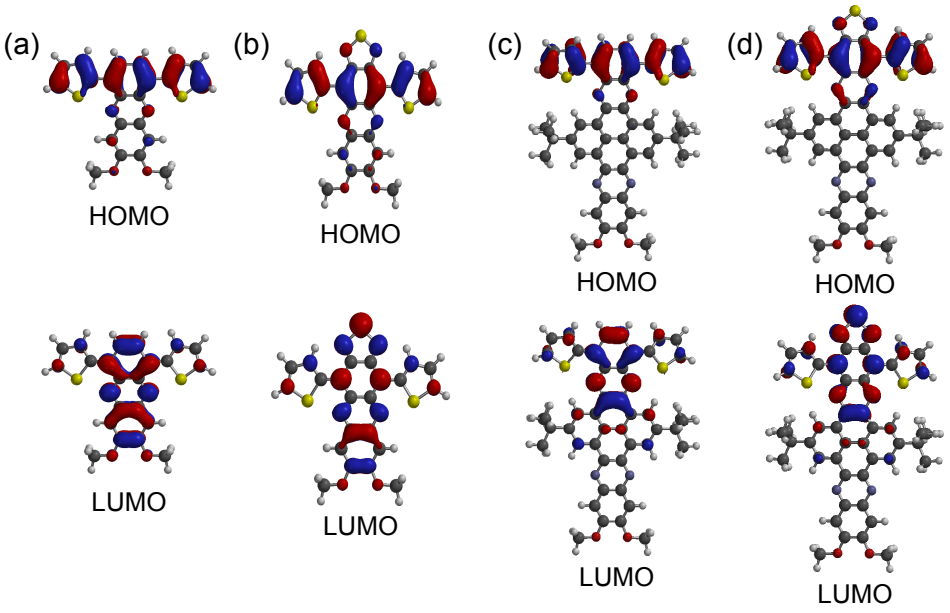

Figure 2.7. Orbital diagrams of HOMO and LUMO: (a) **P-TH-OCH$_3$**, (b) **TD-P-TH-OCH$_3$**, (c) **BP-TH-OCH$_3$**, and (d) **TD-BP-TH-OCH$_3$**.

In addition to the π-core modification, we also conducted a computational investigation into the role of the alkoxy and alkyl side groups. Interestingly, when alkyl side groups were substituted in our two smallest systems (**P-TH** and **TD-P-TH**) the LUMO exhibited a decrease in value by approximately 0.2 eV, while the HOMO lowered by approximately 0.1 eV when compared to the alkoxy version. The net impact on the smaller molecules is a slight E_{gap} compression of 0.1 eV when using alkyl as opposed to alkoxy groups. For our larger molecules, the HOMO and LUMO energies were virtually unchanged by the use of either solubilizing side group. An examination of the distribution of the LUMO orbitals illustrates the rationale for this observation. The LUMO orbitals for the smaller systems extend throughout the entire molecular framework. The electron-donating effect of the alkoxy groups by resonance hinders LUMO lowering, and therefore alkyl group is preferential in LUMO lowering. As stated

previously, in our two larger systems, both HOMO and LUMO orbitals did not extend to the solubilizing side groups, and thus unaffected by the choice of alkoxy or alkyl group.

As previously reported computationally, rotation of one thiophene unit in **TD-P-TH** resulted in an increased E_{gap} of approximately 0.40 eV when compared to E_{gap} in the ground state (planar) geometry. Rotating both thiophene units out of the π-core plane by 90° produced an additive effect, increasing ΔE to 2.40eV. In an effort to test the computationally determined suppositions involving HOMO and LUMO for this system, a slightly modified structure was proposed for both theoretical and experimental study. The new molecule (**TD-P-MeTH-Me**) was structurally identical to **TD-P-TH-Me**, but included the addition of a methyl group at the "3" position of both thiophene units, effectively forcing the rings out of the π-core plane. The optimized geometry of this structure at the B3LYP/6-31G* level of theory predicted a dihedral angle of 51° between thiophene and the π-core, with a ΔE value of 1.90 eV. (Figure 2.8)

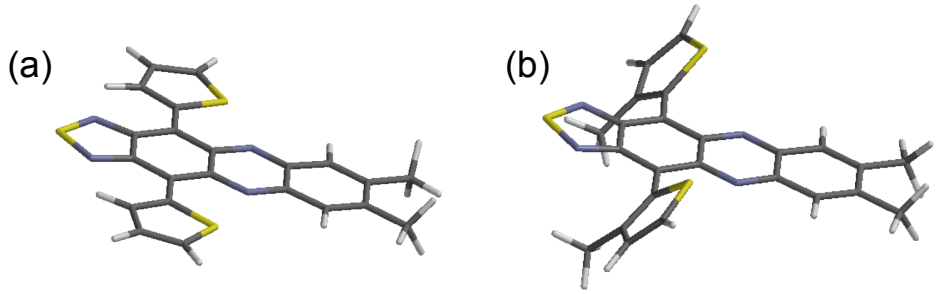

Figure 2.8 Energy-minimized structures of (a) **TD-P-TH-Me** and (b) **TD-P-MeTH-Me**.

2.3.4 Assembly Properties

To test the assembly properties of the **PA-TH**s, cast films from $CHCl_3$ solutions were prepared by slow evaporation onto glass slides. The films produced were characterized by polarized optical microscopy. **P-TH-OC10** and **P-TH-C10** had good solubility in $CHCl_3$ and easily produced uniform cast films of 1D fibers (ca. 500 nm in width) from $CHCl_3$ solutions as seen in Figure 2.9. Despite having more limited solubility, diluted solutions of **BP-TH-OC16** in $CHCl_3$ also gave uniform fibers with a width of ca. 1 μm. **TD-BP-TH-OC16** had poor solubility at concentrations capable of producing a film thick enough for visualization under an optical microscope, and therefore other assembly methods were employed. Cast films of **TD-P-TH-C10** and **TD-P-diTH-C10** did not produce any fibers, rather large leaf like crystals were formed. Despite the assembly method used **TD-P-MeTH-C10** did not display any defined structures.

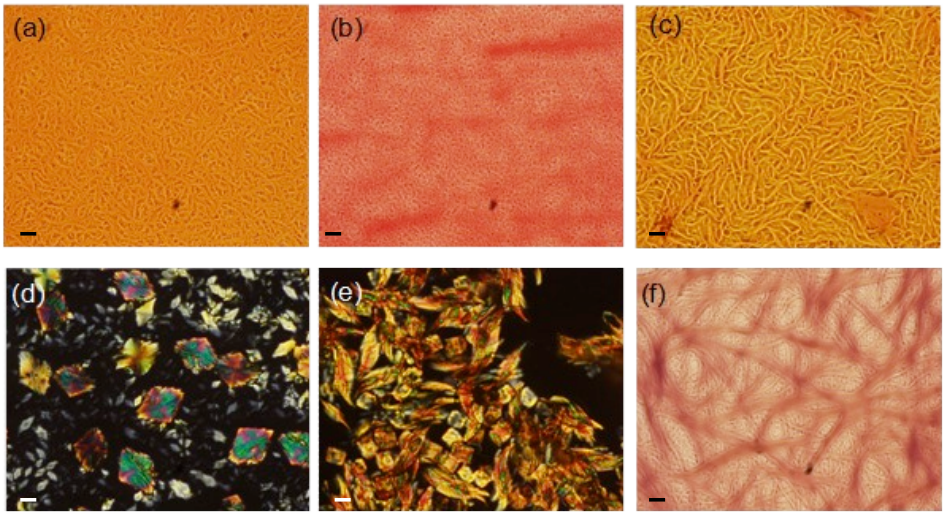

Figure 2.9. Optical micrographs of cast films: (a) **P-TH-OC10** (8 mg / mL $CHCl_3$), (b) **P-TH-C10** (15.3 mg / mL TCE), (c) **BP-TH-OC16** (4mg / mL $CHCl_3$), (d) **TD-P-TH-C10** (cross-polarized) (7 mg / mL $CHCl_3$), (e) TD-P-diTH-C10 (cross polarized) (10^{-5}M $CHCl_3$) and (f) **TD-BP-TH-OC16** (2 mg / mL hot $CHCl_3$, cooled to RT, fibrous precipitate). Scale bars: 10 μm.

Precipitates formed from concentrated $CHCl_3$ solutions of **BP-TH-OC16** and **TD-BP-TH-OC16** were placed on a glass slide and observed under POM. Both compounds showed dense fiber formation. A partial gel was also observed in the case **TD-BP-TH-OC16**. Organogelation studies were not preformed due to the remarkable fibers already formed by simple precipitation. A PT method was used to further study the assembly of **TD-BP-TH-OC16** and the resulting precipitates were characterized using a transmission electron microscope (TEM). TEM was also used to characterize fibers formed from simple precipitation of **TD-BP-TH-OC16** as well as **BP-TH-OC16** from a $CHCl_3$ solution. TEM images are show in figure 2.10. It was discovered that the large bundles observed from **TD-BP-TH-OC16** in POM (from both precipitation and PT assembly), where in fact composed of many thinner fibers with a width of ca. 10 nm. Precipitates of **BP-TH-OC16** from $CHCl_3$ showed tape like fibers, with a width of ca. 100 nm.

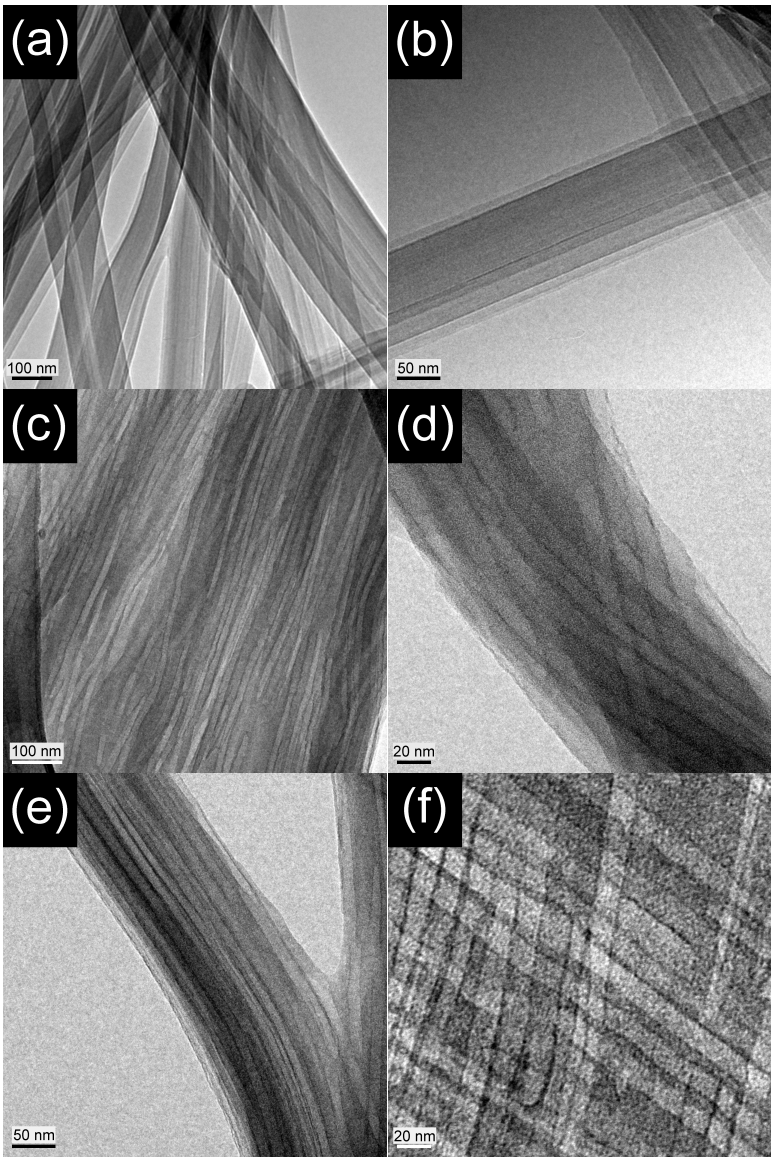

Figure 2.10. TEM images of cast films: (a, b) **BP-TH-OC16** (5.5 mg / mL hot $CHCl_3$, cooled to RT until precipitates formed) and (c, d, e) **TD-BP-TH-OC16** (0.7 mg / mL $CHCl_3$, and then 5mL MeOH slowly added. Left overnight. Purple precipitates), (f) **TD-BP-TH-OC16** (2 mg / mL hot $CHCl_3$, cooled to RT, partial gel).

The absorption behavior of the fibers were further characterized and compared with those in the solution state. Figure 2.11 shows the UV-Vis spectra of cast films of **P-TH-OC10**, **P-TH-C10**, **BP-TH-OC16**, and **TD-BP-TH-OC16** versus a $CHCl_3$ solution. All films had red-shifted absorptions at λ_{max} as well as peaks at longer wavelengths. The

cast film of **P-TH-OC10** shows splitting of λ_{max} with a difference of 20 nm between the two peaks. Shoulder peaks of **P-TH-OC10**, and **P-TH-C10** seen in the thin films, are red shifted by 20 nm and 35 nm, respectively. **BP** based compounds had the most pronounced red-shift at λ_{max} (ca. 20 nm). For both **BP-TH-OC16** and **TD-BP-TH-OC16**, the UV Vis spectra of the cast films showed more definition in the peak structure at longer wavelengths. **TD-BP-TH-OC16** in particular shows peaks at 541 nm, 580 nm, 675 nm, and 733 nm for the cast film whereas the solution state shows high wavelength peaks at 530 nm and 690 nm.

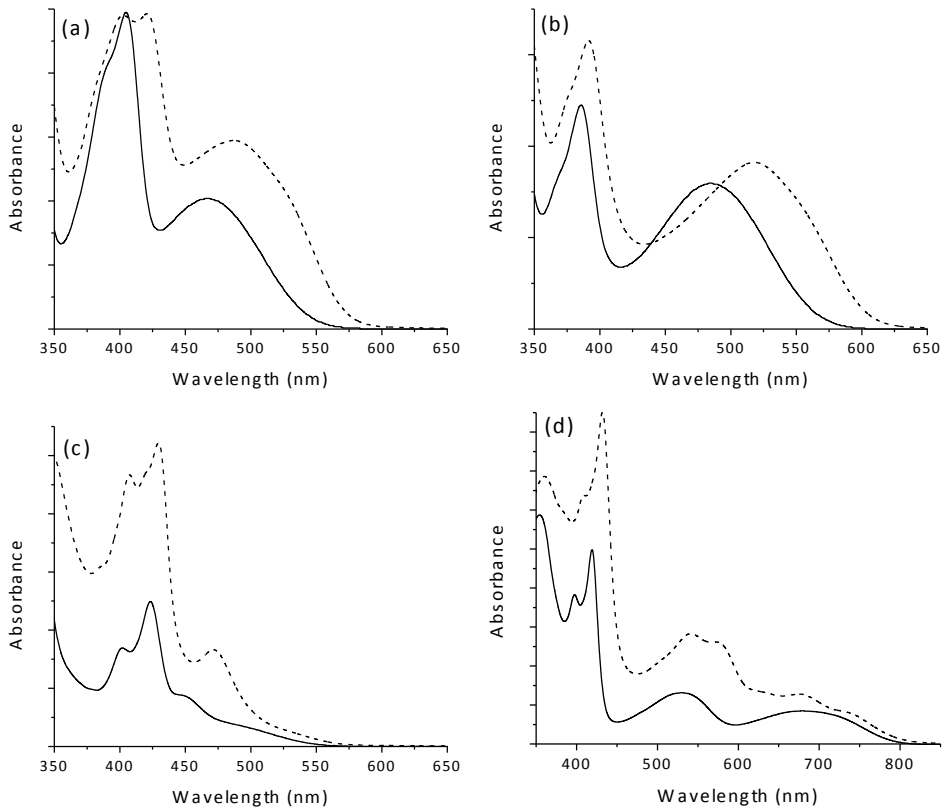

Figure 2.11. UV-Vis absorption spectra of (a) **P-TH-OC10**, (b) **P-TH-C10**, (c) **BP-TH-OC16**, and (d) **TD-BP-TH-OC16** in $CHCl_3$ (solid line) and cast film (dotted line).

2.4 Conclusions

A series of small-molecule donor-acceptor systems have been synthesized and characterized to show independent control of E_{LUMO} and E_{HOMO}, resulting in a compressed E_{gap}. Stille cross coupling between dibromophenazine and 2-(tributylstannyl)thiophene gave **P-TH-OC10** in good yield. For all other compounds, an appropriate diamine compound was prepared via Stille coupling of 2-(tributylstannyl)thiophene with an appropriate intermediate to provide a diamine product for cyclization with various diketo compounds. The compounds prepared using this less direct method, were also obtained in good yields.

With regard to control of E_{LUMO}, extension of the π-core with **TD** further enhanced the electron deficiency of the acceptor part of the molecule resulting in a decreased E_{LUMO}. E_{LUMO} was decreased from -3.32 eV (**TP-P-C0**) to -3.90 eV (**TD-P-TH-C10**). The smaller, **P**-based π-core supported more flexibility in changes to the electronic structure due to the non-disjunctive orbital distribution. Additionally this provided an additional benefit of lowering E_{LUMO} by using less electron rich alkyl side chains rather than alkoxy side chains on the **P** π-core as demonstrated with **P-TH-OC10** and **P-TH-C10**. A difference of 0.15 eV was observed in this case.

Furthermore, it was also shown that the planarity of the molecule plays a crucial role in the control of E_{HOMO}. Extensive theoretical evaluations made on the effects of the dihedral angle on HOMO were supported experimentally when a methyl substituent was introduced to the thiophene unit (**TD-P-MeTH-C10**). This bulky substituent prohibits a planar structure, and a decrease in E_{HOMO} of 0.17 eV was observed with this structural variation.

Ultimately, our goal was to obtain low E_{gap} compounds by independent control of E_{LUMO} and E_{HOMO}. **TD-P-diTH-C10** showed a very impressive E_{gap} of 1.21 eV. The addition of an extra thiophene unit increased E_{HOMO} by 0.18 eV, compared E_{HOMO} of **TD-P-TH-C10**. E_{LUMO} was only lowered by 0.04 eV in this case.

All compounds with the exception of **TD-P-TH-C10**, **TD-P-diTH-C10**, and **TD-P-MeTH-C10** demonstrated the ability to assemble into 1D structures by slow evaporation to a thin film, and/or by a PT method. These fibers were able to be characterized by POM, and TEM. Amazingly, **TD-BP-TH-OC16** forms uniform fibers with a width of ca. 10nm.

APPENDIX & SUPPORTING INFORMATION

LIST OF ABBREVIATIONS

HOMO	Highest Occupied Molecular Orbital
LUMO	Lowest Unoccupied Molecular Orbital
1D	One dimensional
NMR	Nuclear Magnetic Resonance
CV	Cyclic Voltammetry
NBS	N-bromosuccimide
$CDCl_3$	Deuterated chloroform
TCE	Trichloroethane
THF	Tetrahydrofuran
POM	Polarized Optical Microscopy
TEM	Transmission Electron Microscopy
NC-AFM	Non Contact-Atomic Force Microscopy
XRD	X-ray diffraction
T_{gel}	Gelling Temperature
CGC	Critical Gel Concentration
TD	Thiadiazole
TH	Thiophene
PA	Pyrazine-acene

System I Supporting Information.

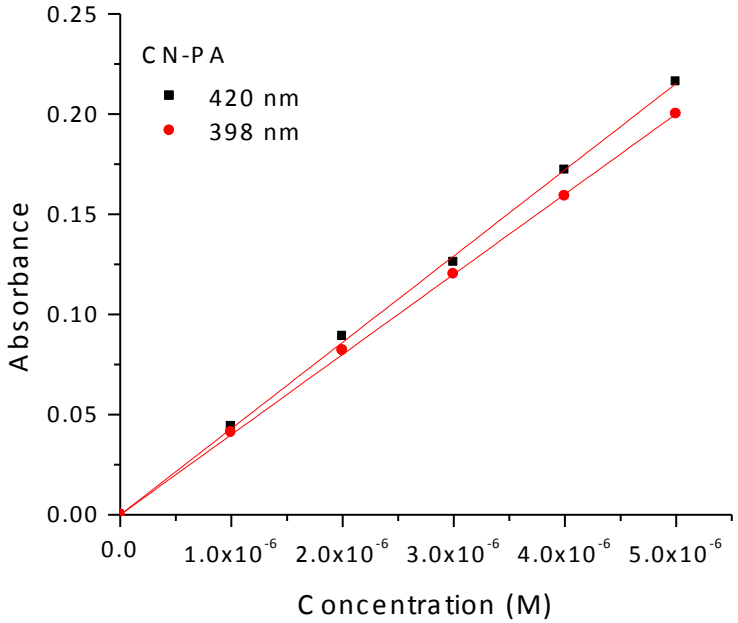

Figure S1. Beer Plot of **CN-PA** in $CHCl_3$

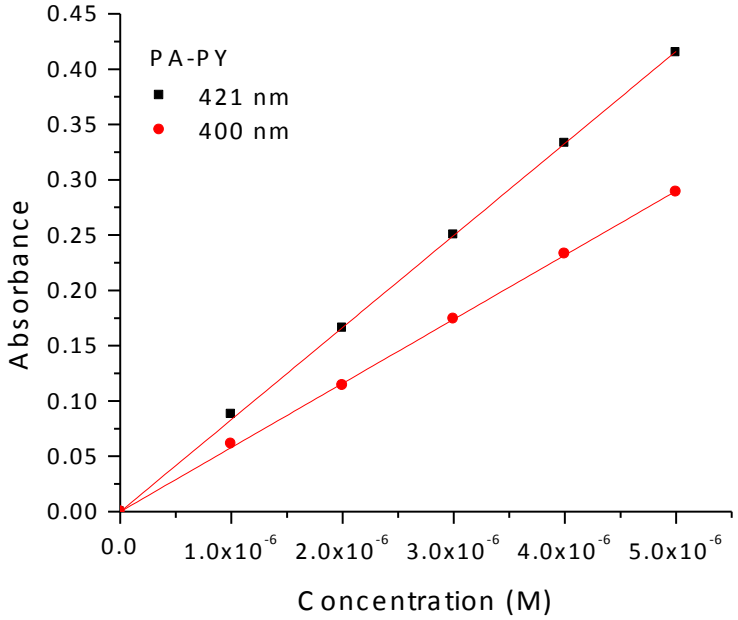

Figure S2. Beer Plot of **PA-PY** in $CHCl_3$

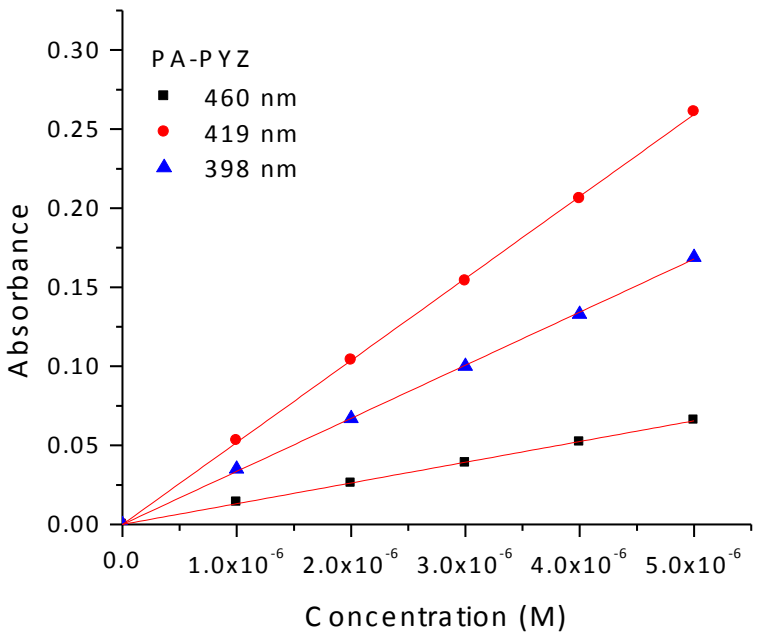

Figure S3. Beer Plot of **PA-PYZ** in $CHCl_3$

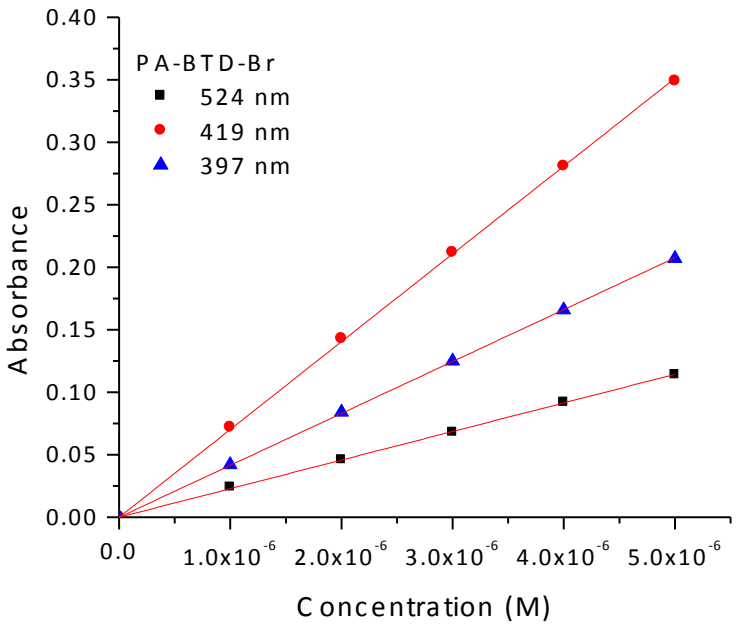

Figure S4. Beer Plot of **PA-BTD-Br** in $CHCl_3$

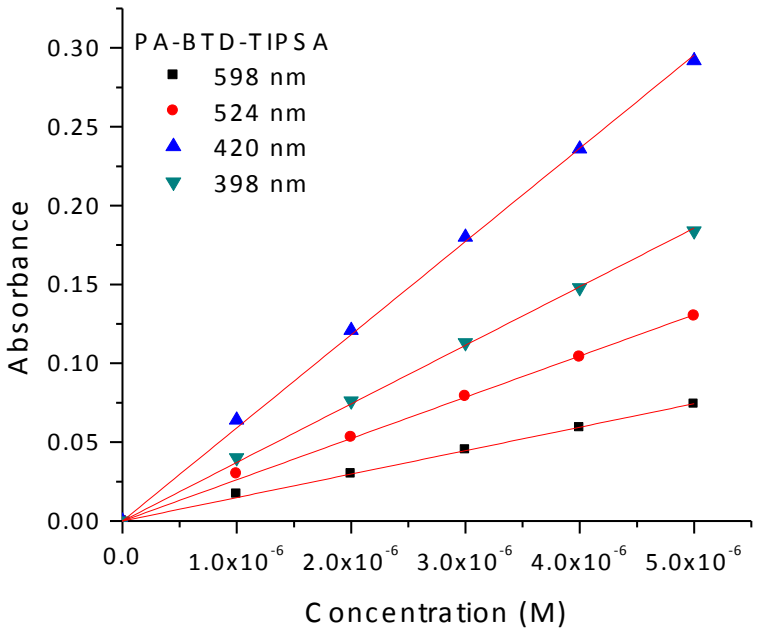

Figure S5. Beer Plot of **PA-BTD-TIPSA** in $CHCl_3$

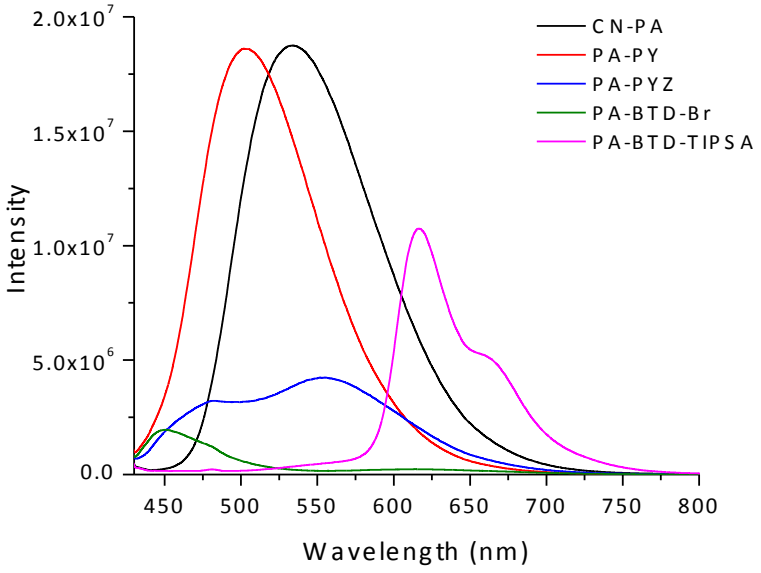

Figure S6. FL spectra of System I. 10^{-7}M in $CHCl_3$. Excitation: 420 nm

System II Supporting Information.

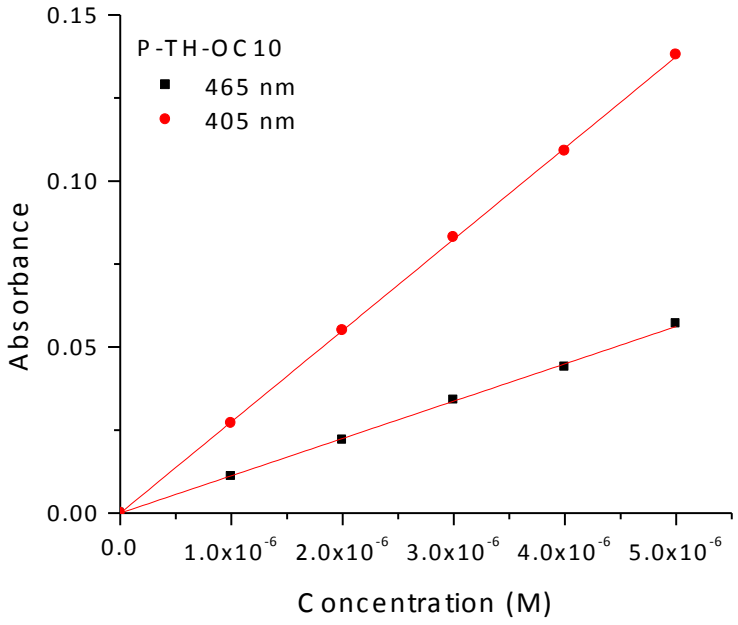

Figure S7. Beer Plot of **P-TH-OC10** in $CHCl_3$

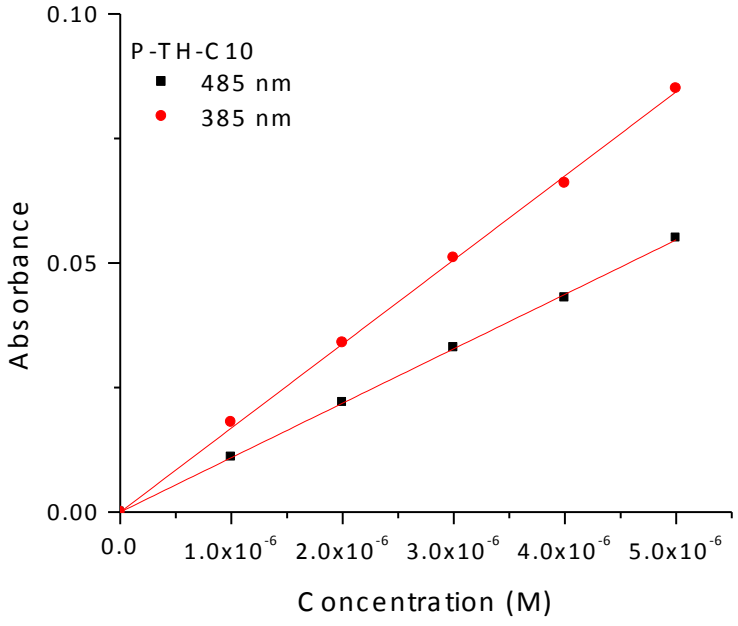

Figure S8. Beer Plot of **P-TH-C10** in $CHCl_3$

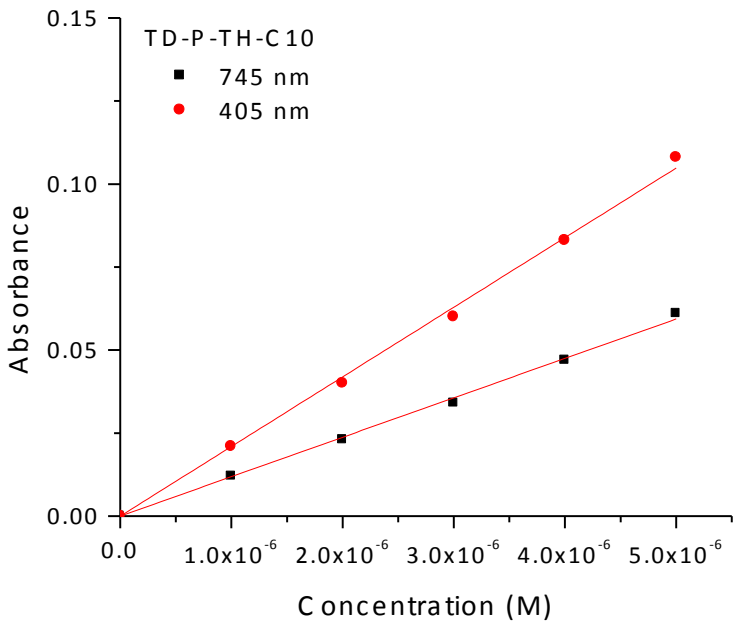

Figure S9. Beer Plot of **TD-P-TH-C10** in $CHCl_3$

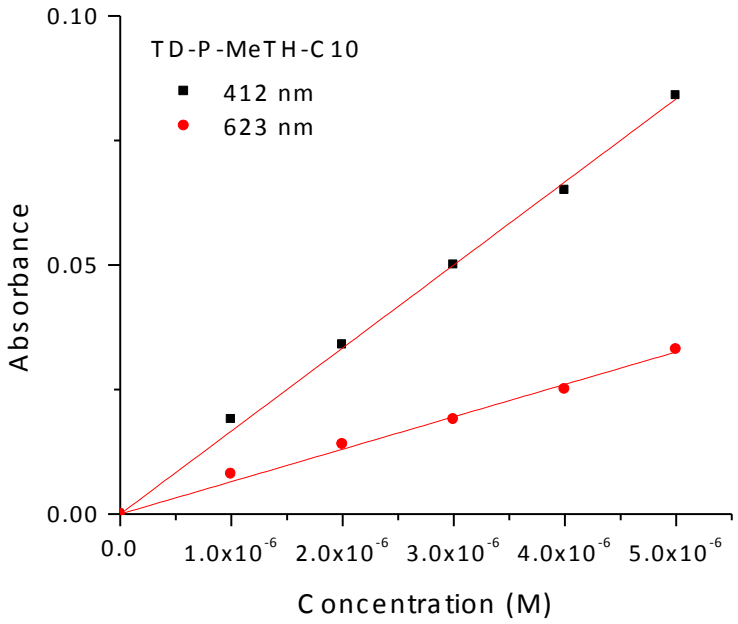

Figure S10. Beer Plot of **TD-P-MeTH-C10** in $CHCl_3$

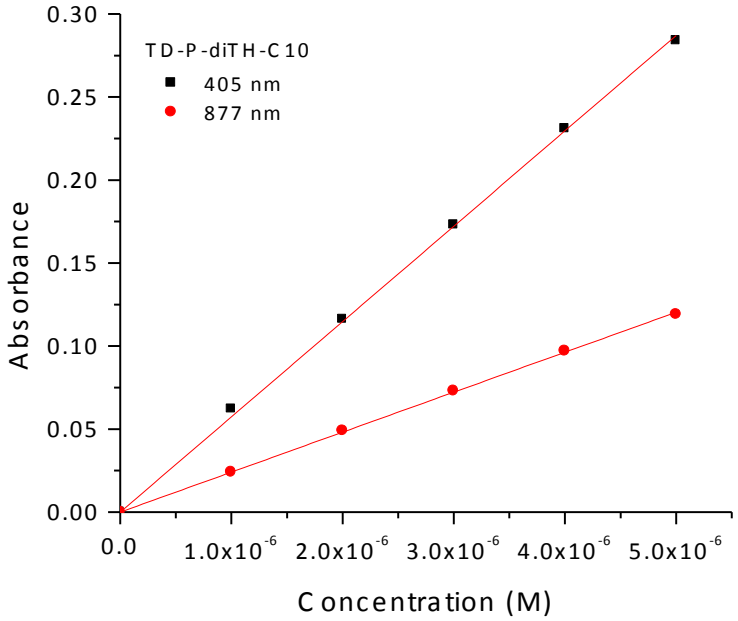

Figure S11. Beer Plot of **TD-P-diTH-C10** in $CHCl_3$

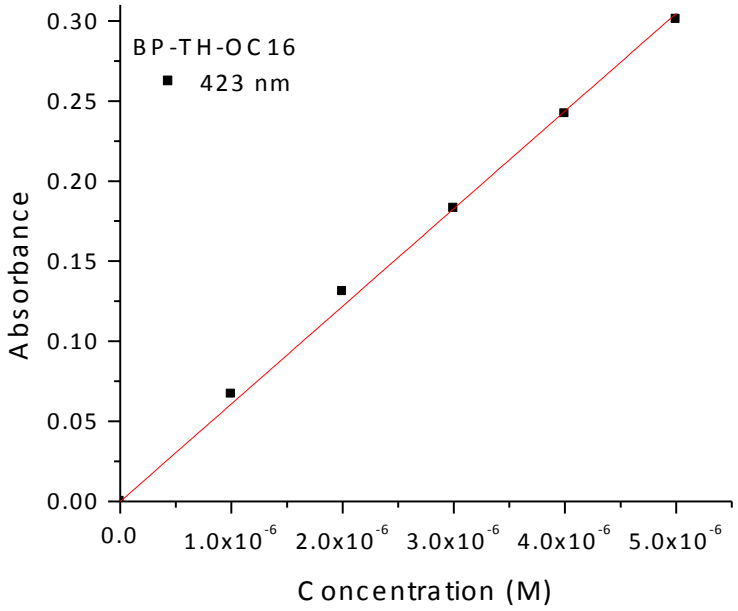

Figure S12. Beer Plot of **BP-TH-OC16** in $CHCl_3$

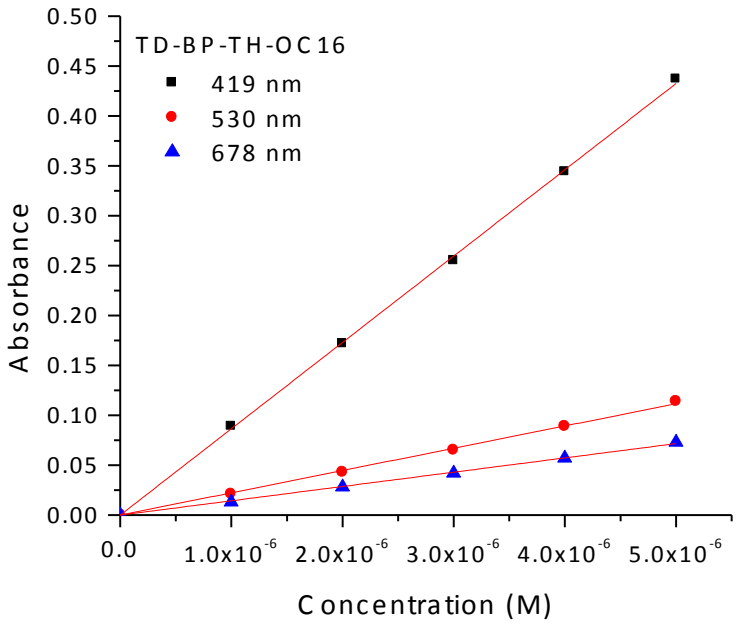

Figure S13. Beer Plot of **TD-BP-TH-OC16** in $CHCl_3$

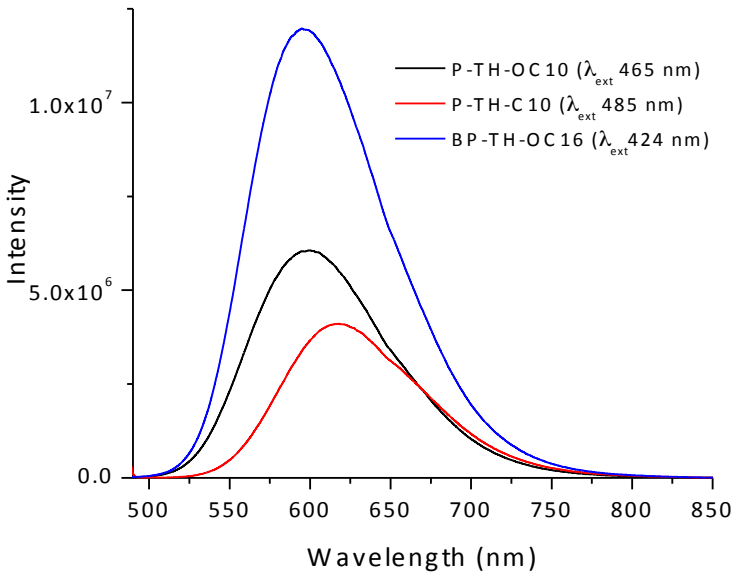

Figure S14. FL spectra for system II. 10^{-6}M $CHCl_3$ solutions.

REFERENCES

1. Jung, B. J.; Tremblay, N. J.; Yeh, M. –L.; Katz, H. E., "Molecular Design and Synthetic Approaches to Electron-Transporting Organic Transistor Semiconductors" *Chem. Mater.* **2011**, *23*, 568–582.
2. Kulkarni, A. P.; Tonzola, C. J.; Babel, A.; Jenekhe, S. A., "Electron Transport Materials for Organic Light-Emitting Diodes" *Chem. Mater.* **2004**, *16*, 4556–4573.
3. Zoombelt, A. P.; Fonrodona, M.; Wienk, M. M.; Sieval, A. B.; Hummelen, J. C.; Janssen, R. A., "Photovoltaic Performance of an Ultrasmall Band Gap Polymer" *J. Org. Lett.* **2009**, *11*, 903–906.
4. Beaujuge, P. M.; Fréchet, J. M. J., "Molecular Design and Ordering Effects in π-Functional Materials for Transistor and Solar Cell Applications" *J. Am. Chem. Soc.* **2011**, *133*, 20009–20029.
5. Zhou, H.; Yang, L.; You, W., "Donor-Acceptor Polymers Incorporating Alkylated Dithienylbenzothiadiazole for Bulk Heterjunction Solar Cells: Pronounced Effect of Positioning Alkyl Chains" *Macromolecules* **2012**, *45*, 607–632.
6. Nishida, J. –I.; Naraso; Murai, S.; Fujiwara, E.; Tada, H.; Tomura, M.; Yamashita, Y., "Preparation, Characterization, and FET Properties of Novel Dicyanopyrazinoquinoxaline Derivatives" *Org. Lett.* **2004**, *6*, 2007-2010.
7. Gao, B.; Wang, M.; Cheng, Y.; Wang, L.; Jing, X.; Wang, F., "Pyrazine-Containing Acene-Type Molecular Ribbons with up to 16 Rectilinearly Arranged Fused Aromatic Rings" *J. Am. Chem. Soc.*, **2008**, *130*, 8297-8306.
8. Richards, G.J.; Hill, J.P.; Subbaiyan, N.K.; D'Souza, F.; Karr, P.A.; Elsegood, M.R.J.; Teat, S.J.; Mori, T.; Ariga, K., "Pyrazinacenes: Aza Analogues of Acenes" *J. Org. Chem.*, **2009**, *74*, 8914-8923.
9. Dallos, T.; Hamburger, M.; Baumgarten, M., "Thiadiazoloquinoxalines: Tuning Physical Properties through Smart Synthesis" *Org. Lett.*, **2011**, *13*, 1936-1939.
10. Nietfeld, J. P.; Schwiderski, R. L.; Gonnella, T. P.; Rasmussen, S. C., "Structural Effects on the Electronic Properties of Extended Fused-Ring Thieno[3,4,*b*]pyrazine Analogues" *J. Org. Chem.*, **2011**, *76*, 6383-6388.
11. Bunz, U. H. F., "N-Heteroacenes" *Chem.–Eur. J.,* **2009**, *15*, 6780-6789.

12. Richards, G. J.; Hill, J. P.; Okamoto, K.; Shundo, A. ; Akada, M.; Elsegood, M. R. J.; Mori, T.; Ariga, K., "Diverse Self-Assembly in Soluble Oligoazaacenes: A Microscopy Study" *Langmuir*, **2009**, *25*, 8408-8413.
13. Bunz, U. H. F., "The larger N-heteroacenes" *Pure Appl. Chem*., **2010**, *82*, 953-968.
14. Richards, G. J.; Hill, J. P.; Mori, T.; Ariga, K., "Putting the 'N' in ACENE: Pyrazinacenes and their structural relatives" *Org. Biomol. Chem*., **2011**, *9*, 5005-5017.
15. Tverskoy, O.; Rominger, F.; Peters, A.; Jimmel, H.-J.; Bunz, U. H. F., "An efficient Synthesis of Tetraazapentacenes" *Angew. Chem. Int. Ed*., **2011**, *50*, 3557-3560.
16. Demanze, F.; Cornil, J.; Garnier, F.; Horowitz, G.; Valat, P.; Yassar, A.; Lazzaroni, R.; Brédas, J.-L., "Tuning of the Electronic and Optical Properties of Oligothiophenes via Cyano Substitution: A Joint Experimental and Theoretical Study" *J. Phys. Chem. B,* **1997**, *101*, 4553-4558.
17. Yassar, A.; Demanze, F.; Jaafari, A.; Idrissi, M. E.; Coupry, C., "Cyano-Substituted Oligothiophenes: A New Approach to n-Type Organic Semiconductors" *Adv. Funct. Mater.,* **2002**, *12*, 699-708.
18. Pappenfus, T. M.; Burand, M. W.; Janzen, D. E.; Mann, K. R., "Synthesis and Characterization of Tricyanovinyl-Capped Oligothiophenes as Low-Band-Gap Organic Materials" *Org. Lett.,* **2003**, *5*, 1535-1538.
19. Kuo, M.-Y.; Chen, H.-Y.; Chao, I., "Cyanation: Providing a Three-in-One Advantage for the Design of n-Type Organic Field-Effect Transistors" *Chem. Eur. J.,* **2007**, *13*, 4750-4758.
20. Lim, Y.-F.; Shu, Y.; Parkin, S. R.; Anthony, J. E.; Malliaras, G. G., "Soluble n-Type Pentacene Derivatives as Novel Acceptors for Organic Solar Cells" *J. Mater. Chem*., **2009**, *19*, 3049-3056.
21. Anthony, J. E., "Small-Molecule, Nonfullerene Acceptors for Polymer Bulk Heterojunction Organic Photovoltaics" *Chem. Mater*., **2011**, *23*, 583-590.
22. Usta, H. ; Facchetti, A. ; Marks, T. J., "n-Channel Semicondutor Materials Design for Organic Complementary Circuits" *Acc. Chem. Res*. **2011**, *44*, 501-510.

23. McGrath, K.K.; Jang, K.; Robins, K.A.; Lee, D.-C., "Substituent Effect on the Electronic Properties and Morphologies of Self-Assembling Bisphenazine Derivatives" *Chem. –Eur. J.*, **2009**, *15*, 4070-4077.
24. Robins, K.A.; Jang, K.; Cao, B.; Lee, D.-C., "Tuning the Electronic Properties of Phenazine and Bisphenazine Derivatives: a Theoretical and Experimental Investigation" *Phys. Chem. Chem. Phys*., **2010**, *12*, 12727-12733.
25. Heidenhain, S. B.; Sakamoto, Y. ; Suzuki, T.; Miura, A.; Fujikawa, H.; Mori, T.; Tokito, S. ; Taga, Y., "Perfluorinated Oligo(p-phenylene)s: Efficient n-Type Semiconductors for Organic Light-Emitting Diodes" *J. Am. Chem. Soc.,* **2000**, *122*, 10240-10241.
26. Moon, H.; Zeis, R.; Borkent, E.-J.; Besnard, C.; Lovinger, A. J.; Siegrist, T. ; Kloc, C. ; Bao, Z., "Synthesis, Crystal Structure, and Transistor Performance of Tetracene Derivatives" *J. Am. Chem. Soc.,* **2004**, *126*, 15322-15323.
27. Schmidt, R.; Ling, M. M.; Oh, J. H.; Winkler, M.; Könemann, M.; Bao, Z. ; Würther, F., "Core-Fluorinated Perylene Bisimide Dyes: Air Stable n-channel Organic Semiconductors for Thin Film Transistors with Exceptionally High On-to-Off Current Ratios" *Adv. Mater.,* **2007**, *19*, 3692-3695.
28. Tang, M. L.; Oh, J. H.; Reichardt, A. D.; Bao, Z., "Chlorination: A General Route toward Electron Transport in Organic Semiconductors" *J. Am. Chem. Soc*., **2009**, *131*, 3733-3740.
29. Appleton, A. L.; Brombosz, S. M.; Barlow, S.; Sears, J. S.; Brédas, J.-L.; Marder, S. R.; Bunz, U. H. F., "Effects of Electronegative Substitution on the Optical and Electronic Properties of Acenes and Diazaacenes" *Nat. Commun.,* **2010**, 1-6.
30. Tang, M. L.; Bao, Z., "Halogenated Materials as Organic Semiconductors" *Chem. Mater*., **2011**, *23*, 446-455.
31. Zhou, H.; Yang, L. ; Stuart, A. C.; Price, S. C.; Liu, S.; You, W., "Development of Fluorinated Benzothiadiazole as a Structural Unit for a Polymer Solar Cell of 7% Efficiency" *Angew. Chem*., **2011**, *123*, 3051-3054.
32. Akhtaruzzaman, M.; Tomura, M.; Nishida, J.; Yamashita, Y., "Synthesis and Characterization of Novel Dipyridylbenzothiadiazole and Bisbenzothiadiazole Derivatives" *J. Org. Chem.,* **2004**, *69*, 2953-2958.

33. Anant, P. ; Lucas, N. T.; Jacob, J., "A Simple Route towards the Synthesis of Bisbenzothiadiazole Derivatives" *Org. Lett*., **2008**, *10*, 5533-5536.
34. Appleton, A. L. ; Miao, S.; Brombosz, S. M.; Berger, N. J.; Barlow, S.; Marder, S. R.; Lawrence, B. M.; Hardcastle, K. I.; Bunz, U. H. F., "Alkynylated Aceno[2,1,3]thiadiazoles" *Org. Lett.,* **2009**, *11*, 5222-5225.
35. Omer, K. M. ; Ku, S.-Y.; Cheng, J.-Z.; Chou, S.-H.; Wong, K.- T.; Bard, A. J., "Electrochemsitry and Electrogenerated Chemiluminescence of a Ppirobifluorene-Based Donor (Triphenylamine)-Acceptor(2,1,3-Benzothiadiazole) Molecule and Its Organic Nanoparticles" *J. Am. Chem. Soc*., **2011**, *133*, 5492-5499.
36. Mutkins, K. ; Gui, K. ; Aljada, M.; Schwenn, P. E.; Namdas, E. B.; Burn, P. L.; Meredith, P., "A Solution Processable Fluorine-benothiadiazole Small Molecule for n-type Organic Field-Effect Transistors" *Appl. Phys. Lett*., **2011**, *98*, 153301-153303.
37. Gwinner, M. C.; Brenner, T. J. K.; Lee, J.-K.; Newby, C.; Ober, C. K.; McNeill, C. R.; Sirringhaus, H., "Organic Field-effect Transistors and Solar Cells using Novel High Electron-Affinity conjugated copolymers based on Alkylbenzotriazole and Benzothiadiazole" *J. Mater. Chem*., **2012**, *22*, 4436-4439.
38. Hoeben, F. J. M. ; Jonkheijm, P.; Meijer, E. W. ; Schenning, P. H. J., "About Supramolecular Assemblies of π-Conjugated Systems" *Chem. Rev.,* **2005**, *105*, 1491-1546.
39. Schenning, A. P. H. J.; Meijer, E. W., "Supramolecular Electronics; Nanowires from Self-Assembled π-Conjugated Systems" *Chem. Commun*., **2005**, 3245-3258.
40. Palmer, L. C; Stupp, S. I., "Molecular Self-Assembly into One-Dimensional Nanostructures" *Acc. Chem. Res*., **2008**, *41*, 1674-1684.
41. Zang, L.; Che, Y.; Moore, J. S., "One-Dimensional Self-Assembly of Planar π-conjugated Molecules: Adaptable Building Blocks for Organic Nanodevices" *Acc. Chem. Res*., **2008**, *41*, 1596-1608.
42. Briseno, A. L.; Mannsfeld, S. C. B.; Lu, X.; Xiong, Y.; Jenekhe, S. A.; Bao, Z.; Xia, Y., "Fabrication of Field-Effect Transistors from Hexathiapentacene Single-Crystal Nanowires" *Nano Lett*., **2007**, *7*, 668-675.

43. Briseno, A. L. ; Mannsfeld, S. C. B.; Reese, C.; Hancock, J. M.; Xiong, Y.; Jenekhe, S. A.; Bao, Z.; Xia, Y., "Perylenediimide Nanowires and Their Use in Fabricating Field-Effect Transistors and Complementary Inverters" *Nano Lett*., **2007**, *7*, 2847-2853.
44. Briseno, A. L.; Mannsfeld, S. C. B.; Shamberger, P. J.; Ohuchi, F. S.; Bao, Z.; Jenekhe, S. A.; Xia, Y., "Self-Assembly, Molecular Packing, and Electron Transport in n-type Polymer Semiconductor Nanobelts" *Chem. Mater*., **2008**, *20*, 4712-4719.
45. Lee, D.-C.; Jang, K.; McGrath, K. K.; Uy, R.; Robins, K. A.; Hatchett, D. W., "Self-Assembling Asymmetric Bisphenazines with Tunable Electronic Properties" *Chem. Mater.,* **2008**, *20*, 3688-3695.
46. Perzon, E.; Wang, X., Admassie, S., Inganäs, Anderrson, M.R., "An alternating low band-gap polyfluorene for optoelectronic devices" *Polymer*, **2006**, *47*, 4261-4268.
47. Eldridge, J. E.; Ferry, J. D., "Studies of the Cross-linking Process in Gelatin Gels. III. Dependence of Melting Point on Concentration and Molecular Weight" *J. Phys. Chem*., **1954**, *58*, 992-995.
48. Da Silva Miranda, F.; Signori, A.M.; Vicente, J.; de Souza, B.; Priebe, J.P.; Szpoganicz, B.; Sanches Goncalves, N.; Neves, A., "Synthesis of substituted dipyrido[3,2-a:2',3'-c]phenazines and a new heterocyclic dipyrido[3,2-f:2',3'-h]quinoxalino[2,3-b]quinoxaline]" *Tetrahedron*, **2008**, *64*, 5410-5415.
49. Becke, A.D., "Density-functional thermochemistry. III. The role of exact exchange" *J. Chem. Phys*., **1993**, *98*, 5648-5652.
50. Iyengar, S. S.; Tomasi, J.; Barone, V.; Mennucci, B. ; Cossi, M. ; Scalmani, G. ; Rega, N.; Petersson, G. A. ; Nakatsuji, H.; Hada, M. ; Ehara, M. ; Toyota, K. ; Fukuda, R.; Hasegawa, J. ; Ishida, M. ; Nakajima, T.; Honda, Y.; Kitao, O.; Nakai, H.; Klene, M.; Li, X.; Knox, J. E.; Hratchian, H. P.; Cross, J. B.; Bakken, V.; Adamo, C. ; Jaramillo, J. ; Gomperts, R. ; Stratmann, R. E.; Yazyev, O.; Austin, A. J.; Cammi, R.; Pomelli, C.; Ochterski, J. W.; Ayala, P. Y. ; Morokuma, K.; Voth, G. A.; Salvador, P.; Dannenberg, J. J.; Zakrzewski, V. G.; Dapprich, S.; Daniels, A. D.; Strain, M. C.; Farkas, O. ; Malick, D. K.; Rabuck, A. D.;

Raghavachari, K.; Foresman, J. B.; Ortiz, J. V.; Cui, Q.; Baboul, A. G. ; Clifford, S.; Cioslowski, J.; Stefanov, B. B.; Liu, G.; Liashenko, A.; Piskorz, P. ; Komaromi, I.; Martin, R. L.; Fox, D. J.; Keith, T. ; Al- Laham, M. A.; Peng, C. Y.; Nanayakkara, A. ; Challacombe, M. ; Gill, P. M. W. ; Johnson, B.; Chen, W.; Wong, M. W.; Gonzalez, C.; Pople, J. A., Gaussian, Inc., Wallingford CT, 2004.

51. Spartan '04, Wavefunction, Inc. Irvine, CA (USA).
52. Terech, P.; Weiss, R. G., "Low Molecular Mass Gelators of Organic Liquids and their Properties as Gels" *Chem. Rev.,* **1997**, *97*, 3133-3159.
53. Sangeetha, N. M.; Maitra, U., "Supramolecular gels: Functions and uses" *Chem. Soc. Rev.,* **2005**, *34*, 821-836.
54. Ajayaghosh, A.; Praveen, V., "π-Organogels of Self-Assembled *p*-Phenylenevinylenes: Soft Materials with Distinct Size, Shape, and Functions" *Acc. Chem. Res.,* **2007**, *40*, 644-656.
55. Anthony, J. E.; Facchetti, A.; Heeney, M. ; Marder, S. R.; Zhan, X., "n-Type Organic Semiconductors in Organic Electronics" *Adv. Mater*., **2010**, *22*, 3876-3892.
56. van Mullekom, H.A.M.; Vekeman, J.A.J.M.; Haring, E.E.; Meijer, E.W., "Developments in the chemistry and band gap engineering of donor-acceptor substituted conjugated polymers" *Mater. Sci. Eng.* **2001**, *32*, 1-40.
57. Mishra, A.; Bäuerle, P., "Small Molecule Organic Semiconductors on the Move: Promises for Future Solar Energy Technology" *Angew. Chem. Int. Ed.*, **2012**, *51*, 2020-2067.
58. Brédas, J.L.; Norton, J.E.; Cornil, J.; Coropceanu, V., "Molecular Understanding of Organic Solar Cells: The Challenges" *Acc. Chem. Res.*, **2009**, *42*, 1691-1699.
59. Bundgaard, E.; Krebs, F.C., "Low Band Gap Polymers for Organic Photovoltaics" *Sol. Energ. Mat. Sol. C.*, **2007**, *91*, 954-985.
60. Wudl, F.; Kobayashi, M.; Heeger, A.J., "Poly(isothianaphthene)" *J. Org. Chem.* **1984**, *49*, 3382-3384.
61. Brédas, J.L.; Heeger, A.J.; Wudl, F., "Towards Organic Polymers with Very Small Intrinsic Band Gaps. I. Electronic Structure of Polyisothianaphthene and Derivatives" *J. Chem. Phys.* **1986**, *85*, 4673-4679.

62. Ferraris, J.P.; Lambert, T.L., "Narrow Bandgap Polymers: Poly-4-dicyanomethylene-4H-cyclopenta[2,1-b:3,4-b']dithiophene (PCDM)" *J. Chem. Soc., Chem. Commun.,* **1991**, 1268-1270.
63. Pomerantz, M.; Chaloner-Gill, B.; Harding, L.O.; Tseng, J.J.; Pomerantz, W.J., "Poly(2,3-dihexylthieno[3,4-*b*]pyrazine). A New Processable Low Band-gap Polyheterocycle" *J. Chem. Soc., Chem. Commun.* **1992**, 1672-1673.
64. Toussaint, J.M.; Brédas, J.L., "Theoretical Analysis of the Geometric and Electronic Structure of Small-Band-Gap Polythiophenes: Poly(5,5'-bithiophene methane) and Its Derivatives" *Macromolecules*, **1993**, *26*, 5240-5248.
65. Meng, H.; Wudl, F., "A Robust Low Band Gap Processable n-Type Conducting Polymer Based on Poly(isothianaphthene)" *Macromolecules*, **2001**, *34*, 1810-1816.
66. Kleinhenz, N.; Yang, L.; Zhou, H.; Price, S.C.; You, W., "Low-Band-Gap Polymers That Utilize Quinoid Resonance Structure Stabilization by Thienothiophene: Fine-Tuning of HOMO Level" *Macromolecules*, **2011**, *44*, 872-877.
67. Havinga, E.E.; ten Hoeve, W.; Wynberg, H., "Alternate Donor-acceptor Small-band-gap Semiconducting Polymers; Polysquarines and Polycroconaines" *Synth. Met.*, **1993**, *55*, 299-306.
68. Pandey, L.; Risko, C.; Norton, J.E.; Brédas, J.L., "Donor-Acceptor Copolymers of Relevance for Organic Photovoltaics: A Theoretical Investigation of the Impact of Chemical Structure Modifications on the Electronic and Optical Properties" *Macromolecules*, **2012**, *45*, 6405-6414.
69. Kitamura, C.; Tanaka, S.; Yamashita, Y. "Design of Narrow-Bandgap Polymers. Syntheses and Properties of Monomers and Polymers Containing Aromatic-Donor and *o*-Quinoid-Acceptor Units" *Chem. Mater.* **1996**, *8*, 570-578.
70. Jayakannan, M.; van Hal, P.A.; Janssen, R.A.J. "Synthesis and Structure-Property Relationship of New Donor-Acceptor-Type Conjugated Monomers and Polymers on the Basis of Thiophene and Benzothiadiazole" *J. Polym. Sci. Part A: Polym. Sci.* **2002**, *40*, 251-261.

71. Chen, G.-Y.; Lan, S.-C.; Lin, P.-Y.; Chu, C.-W.; Wei, K.-H. "Synthesis and Characterization of a Thiadiazole/Benzoimidazole-Based Copolymer for Solar Cell Applications" *J. Polym. Sci. Part A: Polym. Chem.* **2010**, *48*, 4456-4464.
72. Becerril, H.A.; Miyaki, N.; Tang, M.L.; Mondal, R.; Sun, Y.S.; Mayer, A.C; Parmer, J.E.; McGehee, M.D.; Bao, Z., "Transistor and solar cell performance of donor-acceptor low bandgap copolymers bearing an acenaphtho[1,2,-*b*]thieno[3,4-*e*]pyrazine (ACTP) motif" *J. Mater. Chem.* **2009**, *19*, 591-593.
73. Mondal,R.; Miyaki, N.; Becerril, H.A.; Norton, J.E.; Parmer, J.; Mayer, A.C.; Tang, M.L.; Brédas, J.-L. McGehee, M.D.; Bao, Z., "Synthesis of Acenaphthyl and Phenanthrene Based Fused-Aromatic Thienopyrazine Co-Polymers for Photovoltaic and Thin Film Transistor" *Chem. Mater.* **2009**, *21*, 3618-3628.
74. Zhou, H.; Yang, L.; You, W., "A Tale of Current and Voltage: Interplay of Band Gap and Energy Levels of Conjugated Polymers in Bulk Heterojunction Solar Cells" *Macromolecules*, **2010**, *43*, 10390-10396.
75. Beaujuge, P.N.; Jegadesan, S.; Choudhury, K.R.; Ellinger, S.; McCarley, T.D.; So, F.; Reynolds, J.R., "Green Dioxythiophene-Benzothiadiazole Donor-Acceptor Copolymers for Photovoltaic Device Applications" *Chem. Mater.*, **2010**, *22*, 2093-2106.
76. Lloyd, M.T.; Anthony, J.E.; Malliaras, G.G., "Photovoltaics from Soluble Small Molecules" *Mater. Today*, **2007**, *10*, 34-41.
77. Mikroyannidis, J.A.; Tsagkournos, D.V.; Sharma, S.S.; Vijay, Y.K.; Sharma, G.D., "Conjugated Small Molecules with Broad Absorption Containing Pyridine and Pyran Units: Synthesis and Application for Bulk Heterojunction Solar Cells" *Org. Electron*., **2010**, *11*, 2045-2054.
78. McCullough, R.D., "The Chemistry of Conducting Polythiophenes" *Adv. Mater.* **1998**, *10*, 93–116.
79. Mondal, R.; Becerril, H.A.; Verploegen, E.; Kim, D.; Norton, J.E.; Ko, S.; Miyaki, N.; Lee, S.; Toney, M.F.; Brédas, J.-L.; McGehee, M.D.; Bao, Z., "Thiophene-rich fused-aromatic thienopyrazine acceptor for donor-acceptor low band-gap polymer for OTFT and polymer solar cell applications." *J. Mater. Chem.*, **2010**, *20*, 5823-5834.

80. Ao, C.; Zhang, Y. Ng, M.-K., "Derivatives of 4,9-Dihydro-*s*-indaceno[1,2-*b*:5,6-*b'*]dithiophene-4,9-dione: Synthesis and Properties" *J. Org. Chem.* **2007**, *72*, 6364-6371.
81. Henson, Z.B.; Welch, G.C.; van der Poll, T.; Bazan, G.C., "Pyridalthiadiazol-Based Narrow Band Gap Chromophores" *J. Am. Chem. Soc.* **2012**, *134*, 3766-3799.
82. Chen, G.-Y.; Lan, S.-C., Wei. K.-H., "Synthesis and characterization of a Thiadiazole/Benzoimidazole-Based Copolymer for Solar Cell Applications" *J. Poly. Sci., Part A: Poly. Sci.* **2010**, *48*, 4456-4464.
83. Guthrie, D. A.; Tovar, J.D., "Conformation as a Protecting Group: A Regioselective Aromatic Bromination En Route to Complex π-Electron Systems" *Org. Lett.* **2008**, *10*, 4323-4326.
84. Roquet, S.; Leriche, P.; Perepichka, I.; Jousselme, B.; Levillain, E.; Frére, P.; Roncali, J., "3,4-Phenylenedioxythiophene (PheDOT): a Novel Platform for the Synthesis of Planar Substituted π-donor Conjugated Systems" *J. Mater. Chem.*, **2004**, *14*, 1396-1400.
85. Zhu, S.S.; Swager, T.M., "Conducting Polymetallorotaxanes: Metal Ion Mediated Enhancements in Conductivity and Charge Localization" *J. Am. Chem. Soc.* **1997**, *119*, 12568-12577.
86. Lee, D.-C.; Cao. B. Jang, K.; Forster, P. M., "Self-assembly of halogen substituted phenazines" *J. Mater. Chem.* **2010**, *20*, 867-873.
87. Tsubata, Y.; Suzuki, T.; Yamashita, Y.; Mukai, T.; Tsutomu, M., "Tetracyanoquinodimethans Fused with 1,2,5-Thiadiazole and Pyrazine Units" *Heterocycles* **1992**, *33*, 337-348.
88. Réthoré, C.; Madalan, A.; Fourmigué, M.; Canadell, E.; Lopes, E. B.; Almeida, M.; Clérac, R.; Avarvari, N., "O-S vs. N-S intramolecular nonbonded interactions in neutral and radical cation salts of TTF-oxazoline derivatives: synthesis, theoretical investigations, crystalline structures, and physical properties" *New. J. Chem.* **2007**, *31*, 1468-1483.

89. Cozzolino, A. F.; Vargas-Baca, I.; Mansour, S.; Mahmoudkhani, A. H., "The Nature of Supramolecular Association of 1,2,5-Chalcogenadiazoles" *J. Am. Chem. Soc*. **2005**, *127*, 3184-3190.

VITA

Graduate College

University of Nevada, Las Vegas

Lacie V. Brownell

Degrees:

Bachelor of Science in Biochemistry, 2008
University of Nevada- Las Vegas
Las Vegas, NV 89154

Publications:

1. **Lacie V. Brownell**, Kyoungmi Jang, Kathleen Robins, Ich Tran, Clemens Heske, and Dong-Chan Lee; "Controlling the Electron-Deficiency of Self-Assembling Pyrazine-Acenes: A collaborative Experimental and Theoretical Investigation" *Physical Chemistry, Chemical Physics*, **2013**, Accepted.
2. Kyoungmi Jang, **Lacie V.Brownell**, Paul M.Forster, and Dong-Chan Lee; "Self-Assembly of Pyrazine-Containing Tetrachloroacenes" Langmuir, **2011**, 27, 14615-14620.
3. **Lacie V. Brownell**, Jihoon Shin, and Chulsung Bae; "Synthesis of Polar Block Grafted Syndiotactic Polystyrenes via a Combination of Iridium-Catalyzed Activation of Aromatic C-H Bonds and Atom Transfer Radical Polymerization" *Journal of Polymer Science Part A: Polymer Chemistry*, **2009**, *47*, 6655-6667.
4. Tae Soo Jo, Coreen H. Ozawa, Bryce R. Eagar, **Lacie V. Brownell**, Daehyun Han, and Chulsung Bae; "Synthesis of Sulfonated Aromatic Poly(ether amide)s and Their Application to Proton Exchange Membrane Fuel Cells" *Journal of Polymer Science Part A: Polymer Chemistry*, **2009**, *47*, 485-496.
5. Tae Soo Jo, Meilong Yang, **Lacie V. Brownell**, and Chulsung Bae; "Synthesis of Quaternary Ammonium Ion-Grafted Polyolefins via Activation of Inert C-H Bonds and Nitroxide Mediated Radical Polymerization" *Journal of Polymer Science Part A: Polymer Chemistry*, **2009**, *47*, 4519-4531.
6. Jihoon Shin, Andrew Y. Chang, **Lacie V. Brownell**, Ira O. Racoma, Coreen H. Ozawa, Ho-Yong Chung, Shufu Peng, and Chulsung Bae; "Hydrophilic Graft Modification of a Commercial Crystalline Polyolefin" *Journal of Polymer Science Part A: Polymer Chemistry*, **2008**, *46*, 3533-3545.

Thesis Title: Controlling Electronic Properties of Self-Assembling Pyrazine-Acenes

Thesis Examination Committee:
Chairperson, Dong-Chan Lee, Ph.D.
Committee Member, Kathleen A. Robins, Ph.D.
Committee Member, David W. Hatchett, Ph.D.
Graduate Faculty Representative, Monika Neda, Ph.D.